agriculture

MDPI

Article

The Spatiotemporal Variations in and Propagation of Meteorological, Agricultural, and Groundwater Droughts in Henan Province, China

Huazhu Xue, Ruirui Zhang, Wenfei Luan and Zhanliang Yuan *

School of Surveying and Land Information Engineering, Henan Polytechnic University, Jiaozuo 454000, China; xhz@hpu.edu.cn (H.X.); zhangruirui@home.hpu.edu.cn (R.Z.); luanwf@hpu.edu.cn (W.L.)
* Correspondence: yuan6400@hpu.edu.cn

Abstract: As the global climate changes and droughts become more frequent, understanding the characteristics and propagation dynamics of drought is critical for monitoring and early warning. This study utilized the Standardized Precipitation Evapotranspiration Index (SPEI), Vegetation Condition Index (VCI), and Groundwater Drought Index (GDI) to identify meteorological drought (MD), agricultural drought (AD), and groundwater drought (GD), respectively. Sen's slope method and Mann–Kendall trend analysis were used to examine drought trends. The Pearson correlation coefficient (PCC) and theory of run were utilized to identify the propagation times between different types of droughts. Cross-wavelet transform (XWT) and wavelet coherence (WTC) were applied to investigate the linkages among the three types of droughts. The results showed that, from 2004 to 2022, the average durations of MD, AD, and GD in Henan Province were 4.55, 8.70, and 29.03 months, respectively. MD and AD were gradually alleviated, while GD was exacerbated. The average propagation times for the different types of droughts were as follows: 6.1 months (MD-AD), 4.4 months (MD-GD), and 16.3 months (AD-GD). Drought propagation exhibited significant seasonality, being shorter in summer and autumn than in winter and spring, and there were close relationships among MD, AD, and GD. This study revealed the characteristics and propagation dynamics of different types of droughts in Henan Province, providing scientific references for alleviating regional droughts and promoting the sustainable development of agriculture and food production.

Keywords: drought propagation; meteorological drought; agricultural drought; groundwater drought; groundwater drought index

Citation: Xue, H.; Zhang, R.; Luan, W.; Yuan, Z. The Spatiotemporal Variations in and Propagation of Meteorological, Agricultural, and Groundwater Droughts in Henan Province, China. *Agriculture* **2024**, *14*, 1840. https://doi.org/10.3390/agriculture14101840

Academic Editor: Maria A. Tsiafouli

Received: 29 August 2024
Revised: 17 October 2024
Accepted: 17 October 2024
Published: 18 October 2024

1. Introduction

In recent years, the continuous warming of the global climate has led to frequent occurrences of hydrological extreme events, resulting in increasingly severe meteorological disasters [1]. Among the numerous hydrological extreme events, drought is the most common natural disaster globally and is characterized by high frequency, long duration, wide-ranging impact, and massive economic losses [2]. Since the 20th century, more than 70% of countries worldwide have been threatened by droughts of varying intensities, resulting in an annual average direct economic loss of USD 6 to 8 billion [3]. As a country vulnerable to drought, China incurred agricultural economic losses amounting to CNY 27.2 billion annually, with an average affected crop area exceeding 200,000 km^2 per year [4]. Therefore, drought monitoring and early warning have become focal issues of common concern among the international community and experts from various fields [5].

Drought is a complex cyclical event that has a series of negative impacts on agriculture, hydrological systems, and socioeconomic development [6,7]. It is typically categorized into meteorological drought (MD), agricultural drought (AD), hydrological drought (HD), and socioeconomic drought [8]. Understanding the spatiotemporal evolution characteristics of

water cycle elements at different stages is crucial for studying the formation and development process of drought. There is a close relationship between different types of droughts. The phenomenon where one type of drought propagates to others is recognized as drought propagation [9,10]. MD is usually the driving factor of other droughts. Stemming from insufficient precipitation, MD impacts various aspects of the underlying surface, influencing soil, vegetation, runoff, and groundwater to varying degrees, thereby triggering AD, ecological drought, HD, and groundwater drought (GD) [5,8]. In recent years, some scholars have begun to pay attention to the types of droughts such as GD and ecological drought [11,12]. In a broad sense, GD is a type of HD, and its main characteristics are the continuous reduction in the groundwater level and the reduction in groundwater runoff due to the continuous impact of the reduction in groundwater recharge or the increase in groundwater exploitation [13]. With the increasing frequency and severity of drought, it has become increasingly important to reveal the propagation between different droughts in areas with strong interference from human activities.

Previous studies on drought propagation have predominantly focused on two types of droughts, such as MD and AD [14–16] or MD and HD [17,18]. Moreover, studies have primarily concentrated on the global [19–21], national [22–25], or watershed scale [26–29]. However, studies on the propagation dynamics among multiple types of droughts, such as MD, AD, and GD, are relatively scarce. Moreover, such research is particularly rare in Henan Province, which is not only a major agricultural province but also a crucial grain-producing area in China. Nevertheless, with the increasing frequency of droughts, agricultural production and food security in Henan Province have been severely threatened [30]. Additionally, Henan Province is a typical multi-basin aggregation area, spanning four major river basins: the Hai River, the Yellow River, the Yangtze River, and the Huai River. Due to variations in climate conditions across different basins, the distribution of droughts in Henan Province exhibits complex spatiotemporal differences. Therefore, investigating the occurrence patterns, variation characteristics, and propagation dynamics of droughts in different basin divisions of Henan Province is of significant importance for adapting to climate change, making disaster prevention and mitigation decisions, and ensuring the long-term sustainable development of agriculture and food production in this crucial region.

Given the aforementioned context, the objectives of this study are (1) to identify and quantify the spatiotemporal characteristics of MD, AD, and GD; (2) to analyze the changing trends of these three types of droughts; (3) to elucidate the propagation dynamics of droughts under various climatic conditions in different basins; and (4) to investigate the linkages among the three types of droughts. The findings of this research will contribute to a deeper understanding of the propagation relationships among different types of droughts in Henan Province, providing novel insights for regional drought propagation studies.

2. Materials and Methods

2.1. Study Area

Henan Province (HP) (31°23′ N–36°22′ N, 110°21′ E–116°39′ E) is located in the central plains of China (Figure 1). It has a total land area of 167,000 km^2, stretching approximately 530 km from north to south and 580 km from east to west. The terrain of HP slopes from west to east, bordering Anhui and Shandong provinces to the east, Hebei and Shanxi provinces to the north, Shaanxi Province to the west, and Hubei Province to the south. The climate of HP exhibits significant regional differences between the northern and southern areas. The northern region experiences a temperate continental climate, with summers that are hot and rainy and winters that are cold and dry. In contrast, the southern region has a subtropical monsoon climate, characterized by hot and humid summers and mild and rainy winters. The province has an average annual temperature ranging from 10.5 to 16.7 °C, an annual precipitation between 407.7 and 1295.8 mm, and an annual sunshine duration ranging from 1285.7 to 2292.9 h. Additionally, the frost-free period spans from 201 to 285 days annually. As an important grain-producing region and agricultural province in

China, HP is susceptible to droughts and floods, which is attributed to the differences in the spatiotemporal distribution of precipitation. Therefore, studying the spatiotemporal variation characteristics and propagation mechanisms of droughts in HP plays a crucial role in ensuring national food security.

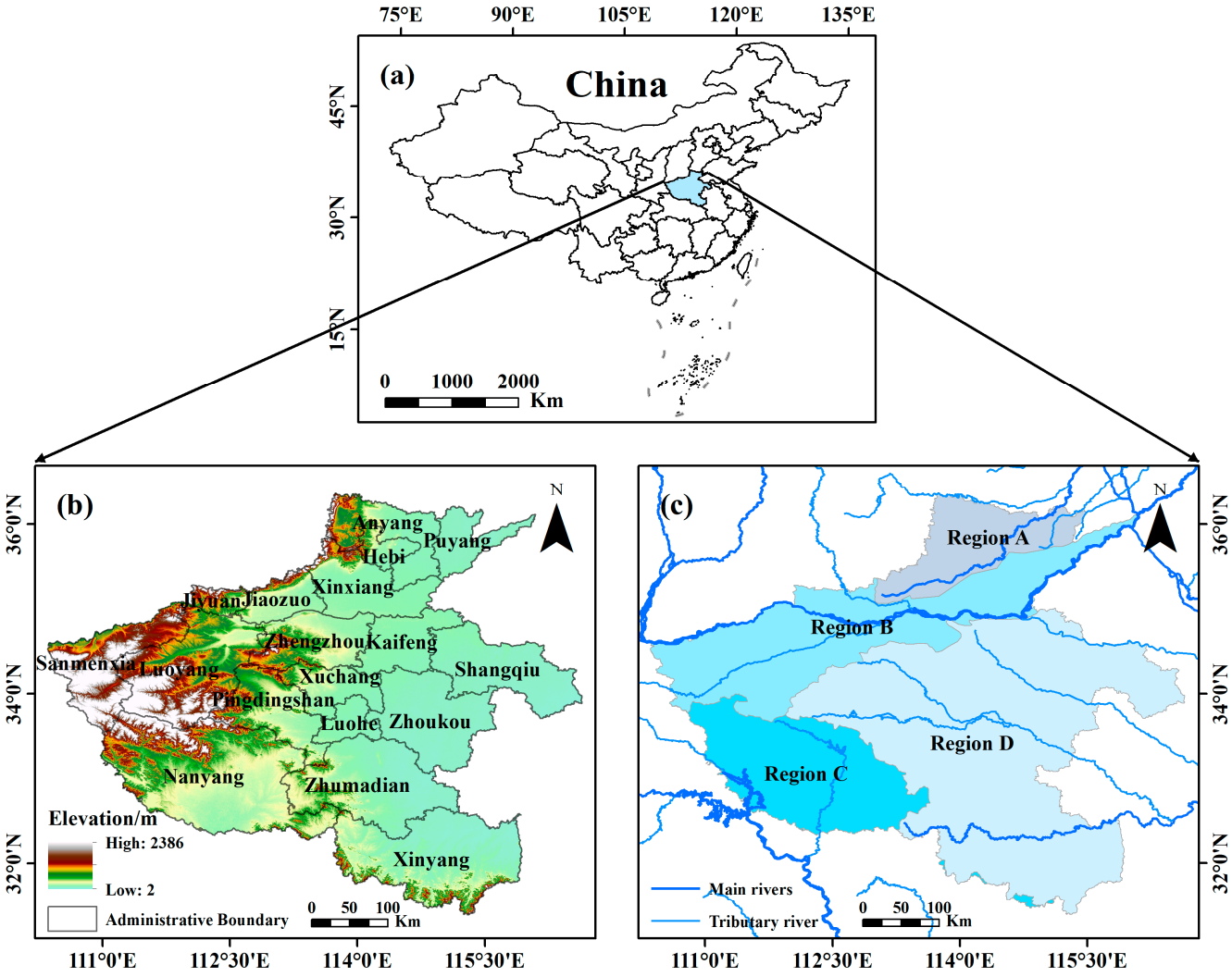

Figure 1. The position of China (**a**), distribution of elevation (**b**), and watershed divisions (**c**) in Henan Province.

To better reveal the variations in different types of droughts and their propagation characteristics in diverse regional environments, HP was partitioned into four subregions based on the watershed position of each region (Region A: Hai River Basin (HARB); Region B: Yellow River Basin (YRB); Region C: Yangtze River Basin (YZRB); and Region D: Huai River Basin (HURB)), as illustrated in Figure 1c.

2.2. Data Description

2.2.1. SPEI Data

In this study, the Standardized Precipitation Evapotranspiration Index database (SPEIbase), Version 2.9 (https://developers.google.com/earth-engine/datasets/catalog/CSIC_SPEI_2_9, accessed on 1 February 2024), was utilized to investigate the variations in MD in HP. The SPEIbase v2.9 provides reliable information on long-term drought globally, with a spatial resolution of 0.5 degrees and a temporal resolution of one month. Moreover, this database offers SPEI time scales ranging from 1 to 48 months, covering the period from

1901 to 2022. In this study, the SPEI datasets were selected for 1 to 24 months in the period 2004–2022, and then bilinear interpolation was employed to interpolate to 0.25 degrees.

2.2.2. MODIS Data

The dataset of the Normalized Difference Vegetation Index (NDVI) used in this study was acquired from MODIS/Terra products (MYD13A2 V6.1) obtained from the website (https://developers.google.com/earth-engine/datasets/catalog/MODIS_061_MYD13A2, accessed on 1 February 2024). This dataset has a spatial resolution of 1 km and a temporal resolution of 16 days, ensuring detailed and frequent monitoring of vegetation dynamics, which was provided by NASA LP DAAC at the USGS EROS Center. For this investigation, the NDVI data from 2004 to 2022 were selected for the computation of the Vegetation Condition Index (VCI). To ensure the spatial coherence of all the experimental data, bilinear interpolation was used to adjust the NDVI data to a spatial resolution of 0.25°.

2.2.3. Global Land Data Assimilation System (GLDAS)

GLDAS is a high-resolution global land simulation system jointly developed by NASA's Goddard Space Flight Center (GSFC) and NOAA's National Centers for Environmental Prediction (NCEP) [31]. This system assimilates satellite data and observational data to generate comprehensive land surface simulations. For this study, groundwater storage data from the GLDAS-2.2 product (https://developers.google.com/earth-engine/datasets/catalog/NASA_GLDAS_V022_CLSM_G025_DA1D, accessed on 1 February 2024), with a spatial resolution of 0.25° and covering the period from 2004 to 2022, were used to calculate the Groundwater Drought Index (GDI).

2.2.4. Auxiliary Data

The DEM data were acquired from the Geospatial Data Cloud (https://www.gscloud.cn/, accessed on 1 February 2024). Temperature data were sourced from ERA5-Land (https://developers.google.com/earth-engine/datasets/catalog/ECMWF_ERA5_LAND_MONTHLY_AGGR, accessed on 2 April 2024), and evapotranspiration data were acquired from the global land surface monthly climate and water balance dataset (https://developers.google.com/earth-engine/datasets/catalog/IDAHO_EPSCOR_TERRACLIMATE, accessed on 2 April 2024). Both the temperature and evapotranspiration data were downloaded and preprocessed using Google Earth Engine (GEE). Detailed information on water resources, reservoir dynamics, and water usage was obtained from the Henan Water Resources Bulletin (https://slt.henan.gov.cn/bmzl/szygl/szygb/, accessed on 2 April 2024). For this study, we collected data on drought-related factors in HP from 2004 to 2022, including precipitation, temperature, evapotranspiration, vegetation, surface water resources, groundwater resources, the storage capacity of major and mid-sized reservoirs, agricultural irrigation water consumption, and total water consumption (including industrial, urban and rural living, environments), to analyze the impact of these factors on drought propagation across different subregions.

2.3. Methods

In this study, the Standardized Precipitation Evapotranspiration Index (SPEI), Vegetation Condition Index (VCI), and Groundwater Drought Index (GDI) were utilized to identify MD, AD, and GD, respectively. The classification levels for these drought indices are presented in Table 1. The trends of different types of droughts were analyzed using Sen's slope method and the Mann–Kendall trend test. The Pearson correlation coefficient and theory of run were employed to identify the propagation time between different types of droughts. The relationships among these three types of droughts were explored using cross-wavelet transform (XWT) and wavelet coherence (WTC). The flowchart of this study is illustrated in Figure 2.

Table 1. Classification of the drought severity levels based on the drought indices.

Drought Severity	SPEI/GDI	VCI
No drought	(−0.5, 0.5)	(50, 100)
Mild drought	(−1.0, −0.5]	(30, 50]
Moderate drought	(−1.5, −1.0]	(20, 30]
Severe drought	(−2.0, −1.5]	(10, 20]
Extreme drought	(−∞, −2.0]	[0, 10]

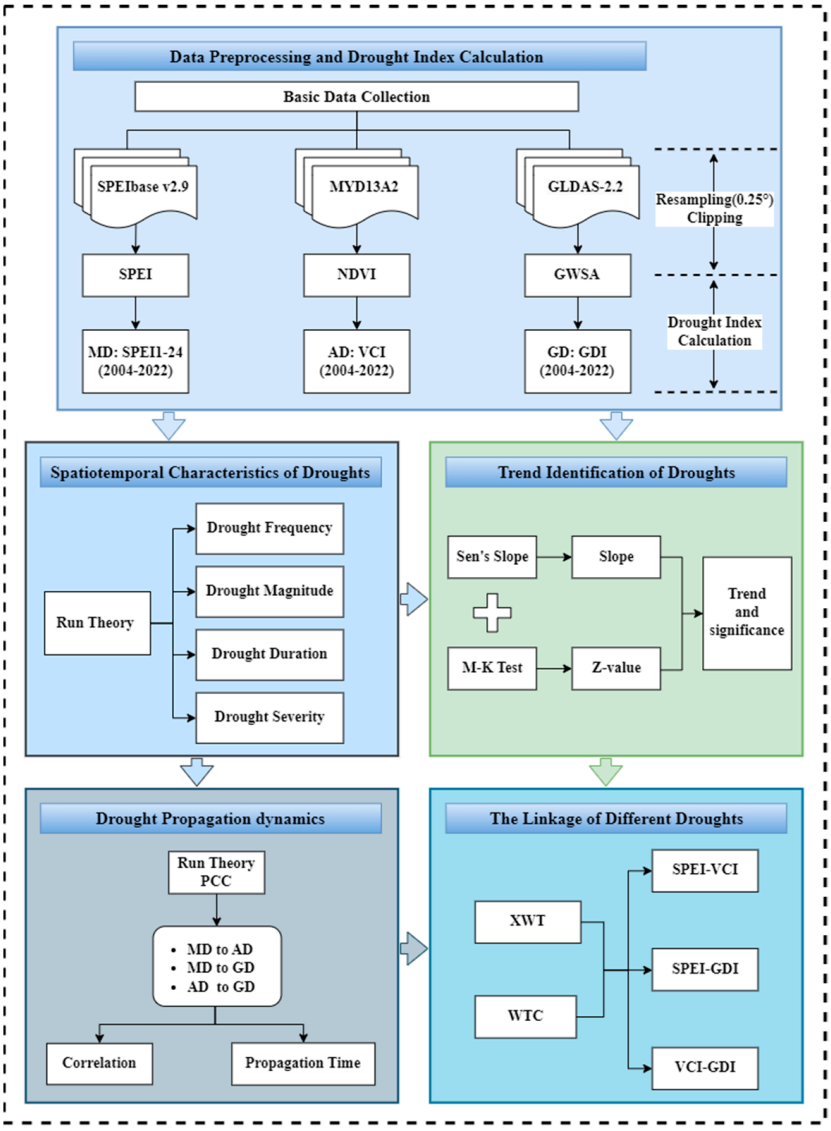

Figure 2. The flowchart of this study.

2.3.1. Drought Indices

Standardized Precipitation Evapotranspiration Index (SPEI)

The SPEI is a meteorological drought index characterized by its multitemporal scale and spatial comparability, developed by Vicente-Serrano et al. [32]. Considering monthly precipitation and potential evapotranspiration, this index is employed to determine the water budget deficit and surplus. In comparison to other meteorological drought indices, the SPEI not only combines the advantages of the Palmer Drought Severity Index (PDSI) and the Standardized Precipitation Index (SPI), but also offers simple and convenient calculations, sensitivity in drought response, and flexibility in time scales. Widely utilized

in meteorological drought research, detailed calculation procedures for this index can be found in Zhu et al. [33].

Vegetation Condition Index (VCI)

The Normalized Difference Vegetation Index (NDVI) has recently been utilized not only to reflect vegetation growth conditions but also as a tool for evaluating drought events by numerous researchers [34–36]. However, the NDVI can only reflect the impact of climate, soil, and hydrological factors on vegetation in isolation and is highly sensitive to geographical environmental conditions, rendering it unsuitable for cross-regional drought monitoring. To overcome this limitation, the VCI was developed based on the NDVI [37]. The VCI can reflect the drought-affected environment resulting from the interaction between vegetation and its growing environment, and accurately characterize the physiological response of vegetation to drought stress, making it suitable for monitoring agricultural drought [38,39]. Additionally, serving as an indicator of crop growth and ground vegetation cover, the VCI can reduce the impact of diverse geographical areas, soil conditions, and ecosystems on vegetation [12,36]. The formula for calculating the VCI is as follows:

$$\mathrm{VCI} = \frac{NDVI_i - NDVI_{min}}{NDVI_{max} - NDVI_{min}} * 100 \quad (1)$$

where $NDVI_i$ is the monthly NDVI value at a specific period i of a particular year; $NDVI_{max}$ and $NDVI_{min}$ are the multiyear maximum NDVI and multiyear minimum NDVI over the study period, respectively. The VCI values range between 0 and 100, and lower VCI values indicate poorer vegetation growth and more severe drought conditions.

Groundwater Drought Index (GDI)

The GDI was proposed based on GRACE data, offering a novel method to assess hydrological drought in regions with limited data availability [40]. It is a normalization-based indicator of groundwater storage (GWS) that evaluates GD by combining the deficits and surpluses of GWS. Recently, this index has been gradually applied to identify GD [13,41,42]. This study drew on the experience of previous studies [43,44], and the GDI was constructed utilizing the GWS data from GLDAS-2.2. The calculation steps of the GDI are as follows:

First, the monthly climatology (M_i) was calculated based on the GWS data. The M_i used here did not refer to climate in the climatological definition, and it was used to remove the effect of monthly variability factors on the GWS. The equation is as follows:

$$M_i = \frac{\sum_1^{n_i} GWS_i}{n_i},\ i = 1, 2, \ldots, 12 \quad (2)$$

where M_i indicates the climatology for month i.

Then, the monthly groundwater storage deviation (GSD_i) was obtained by subtracting the M_i from the GWS_i. This deviation reflects the net variation in groundwater storage. The GSD_i was calculated as follows:

$$GSD_i = GWS_i - M_i \quad (3)$$

Finally, the GDI was calculated as the result of the GSD_i subtracting the mean of the GSD_i ($\overline{X}_{GSD}$) and then dividing it by the standard deviation of the GSD_i (S_{GSD}), as follows:

$$\mathrm{GDI} = \frac{\left(GSD_i - \overline{X}_{GSD}\right)}{S_{GSD}} \quad (4)$$

where the $\overline{X}_{GSD}$ was utilized to mitigate the influence of seasonal variations on the GWS fluctuations.

2.3.2. Theory of Run

The theory of run is a method of time series analysis [45]. It has been widely utilized for the identification of drought events [46]. This approach can identify and analyze various characteristics of drought events, including drought onset and end time, drought duration, drought frequency, drought magnitude, and drought severity [47]. As a threshold-based algorithm, run theory defines drought events as periods during which values consistently fall below a specific drought threshold. According to the drought level classification, −0.5 was set as the threshold of drought in this study. Further, the characteristics of drought were obtained. Details on the theory and computational methods can be found as a reference [48].

2.3.3. Trend Analysis Method

In this paper, Sen's slope and Mann–Kendall trend test were utilized to analyze trends in various drought index series. The combination of Sen's slope and Mann–Kendall trend test can effectively reduce noise interference and accurately determine the significance of serial trends, thereby improving the accuracy of the results.

Sen's Slope

Sen's slope is a robust nonparametric trend estimation method [49]. It has been widely applied in meteorology and hydrology due to its advantages of efficient algorithm calculations and insensitivity to outliers and errors [50]. The calculation of Sen's slope is as follows:

$$\text{Slope} = \text{Median}\left[\frac{x_j - x_i}{j - i}\right], \forall\, 1 \le i \le j \le n \tag{5}$$

where x_i and x_j represent the drought index values at time i and j, respectively. When Slope > 0, the time series shows an increasing trend; conversely, it indicates a decreasing trend.

Mann–Kendall Trend Test

The Mann–Kendall (MK) trend test [51], a nonparametric statistical test method highly recommended by the World Meteorological Organization, was used to detect the significance level of the trend slope [30,52]. The data samples do not need to adhere to a specific distribution, and it is not affected by a small number of outliers. These advantages make it appropriate for analyzing meteorological, hydrological, and other non-normally distributed data. The calculation principle is as follows:

Assume a time series data are $X = (X_1, X_2, \ldots, X_n)$, then the M-K test statistic S is estimated as follows:

$$\text{S} = \sum_{i=1}^{n-1} \sum_{j=i+1}^{n} sgn(X_j - X_i) \tag{6}$$

where

$$sgn(X_j - X_i) = \begin{cases} 1\,, & X_j > X_i \\ 0\,, & X_j = X_i \\ -1\,, & X_j < X_i \end{cases} \tag{7}$$

S follows a normal distribution, and its variance is calculated as follows:

$$\text{Var(S)} = \frac{n(n-1)(2n+5)}{18} \tag{8}$$

The significance of the trend in the time series at a certain confidence interval is tested by calculating the test statistic Z:

$$Z = \begin{cases} \frac{S-1}{\sqrt{Var(S)}}\,, & S > 0 \\ 0\,, & S = 0 \\ \frac{S+1}{\sqrt{Var(S)}}\,, & S < 0 \end{cases} \tag{9}$$

At a given ∂ confidence level, if $|Z| > Z_{1-\partial/2}$, the null hypothesis is rejected. When $|Z|$ is greater than or equal to 1.96 or 2.58, the significance test is passed with a 95% or 99% confidence level, respectively.

2.3.4. Pearson Correlation Coefficient (PCC)

The PCC is a statistical index measuring the linear relationship between variables and is extensively applied in scientific research [53]. It performs well in detecting linear relationships and can effectively capture the propagation relationships between different types of droughts, as well as determine the drought propagation time [2,54]. Before conducting the correlation analysis, we performed a normality test on the SPEI, VCI, and GDI data, which showed that the data for all three drought indices followed a normal distribution. Therefore, this study selected this method to calculate the correlation between the SPEI-n (1, 2, 3, . . ., 24 months) and the VCI or GDI at the 1-month scale, to quantify the propagation time among MD, AD, and GD. The correlation coefficient R is calculated as follows:

$$R = \frac{cov(x, y)}{\sigma_x \sigma_y} \tag{10}$$

where x and y are the time series of the two drought indices at different scales; $cov(x, y)$ is the covariance of the rank variables; and σ_x and σ_y represent the standard deviations of these rank variables.

2.3.5. Cross-Wavelet Transform and Wavelet Coherence Analysis

Cross-wavelet transform (XWT) and wavelet coherence (WTC) are effective approaches applied to test the relationship between two time series. The XWT [55] is a new method merging cross-spectral analysis with wavelet transform, which enhances the ability to test the connections between two time series in both the time and frequency domains [56,57]. XWT has strong signal coupling and discriminative ability, which makes it ideal for investigating the distribution and phase relationships between time series. Defining two time series as X_n and Y_n, the XWT can be expressed as follows:

$$W_{XY}(\alpha, \tau) = C_X(\alpha, \tau) C_Y^*(\alpha, \tau) \tag{11}$$

However, XWT does not perform well in low-energy regions and this problem can be mitigated through the application of WTC [58]. WTC evaluates the correlation between two time series as a function of frequency, and its value varies between 0 and 1 [56]. This method can be interpreted as the decomposition of the correlation coefficient across various scales [59]. After normalizing the wavelet energy of X and Y, the WTC can be calculated by the following equation:

$$R^2(s, t) = \frac{\left| S\left(s^{-1} W_{XY}(s, t)\right) \right|^2}{S\left(s^{-1} |W_X(s, t)|^2\right) \cdot S\left(s^{-1} |W_Y(s, t)|^2\right)} \tag{12}$$

where $R^2(s, t)$ denotes the local correlation coefficient in the time–frequency domain, S represents the smoothing operator, s denotes the scale factor, and t indicates the translation factor. $W_X(s, t)$ and $W_Y(s, t)$ are the wavelet transforms of the series X and Y, respectively.

Additionally, the causal relationship between X and Y can be evaluated by calculating the cross-wavelet phase angle. This is performed by utilizing the circular mean of a set of angles and plotting the confidence interval of the phase difference in the range of 0° to 360° [58]. The calculation of the phase angle is as follows:

$$\theta_{XY}(s, t) = \tan^{-1}\left(\frac{I\left(SW_n^{XY}(s)\right)}{R\left(SW_n^{XY}(s)\right)}\right), \theta_{XY}(s, t) \in [-\pi, \pi] \tag{13}$$

where I and R represent the real and imaginary, respectively. The phase difference is distributed across four quadrants, showing the leading and lagging relationships between the time series X and Y. This is illustrated by the directional arrows in the wavelet coherence power spectrum. Phase arrows pointing left or right indicate whether the two factors are in-phase or out-of-phase, respectively [60].

3. Results

3.1. Spatiotemporal Characteristics of Droughts

3.1.1. Temporal Variations in MD, AD, and GD

Figure 3 illustrates the changes in the SPEI for HP and its different subregions from 2004 to 2022 at scales of 1 to 24 months. As shown in Figure 3a, as the time scale increases, the frequency of droughts is becoming less and less, the drought duration lasts longer and longer, and the drought magnitude is becoming smaller and smaller. The SPEI reflects alternating wet and dry conditions. From 2004 to 2009, the region experienced relatively humid conditions. In 2010, a severe drought occurred, which persisted until 2013. Drought conditions were alleviated from 2014 to 2016, but the years 2017–2018 were characterized by relative dryness. Drought conditions relatively improved from 2019 to 2021, but in 2022, a relatively severe drought reemerged.

The variations in the SPEI-n (n = 1, 2, 3 . . . 24) in different subbasins of HP from 2004 to 2022 are illustrated in Figure 3b–e. Each subregion demonstrated distinctive alternations between wet and dry conditions, aligning closely with the overall trend observed across the entire province. HP was significantly wet during 2004–2009, 2014–2016, and 2019–2021, while it was significantly dry during 2010–2013, 2017–2018, and 2022. However, due to the unique climatic environments within each subbasin, the severity of MD events varied significantly. A comparative analysis among the four subregions revealed that the wet–dry fluctuations in Region A were relatively mild, followed by those in Regions B and D, with Region C exhibiting the most severe drought conditions.

Figure 4 illustrates the changes in the VCI on a monthly scale in HP and its subregions from 2004 to 2022. As shown in Figure 4, the overall trend of the VCI in HP alternated between dry and wet conditions, showing a gradual increase over time. Notably, the region frequently experienced mild to moderate, and even severe droughts, between 2004 and 2013, suggesting that the vegetation drought situation across HP was particularly serious during this period. Conversely, a noticeable reduction in drought occurrence has been observed since 2014. Additionally, compared to the other three regions, Region A exhibited the most significant fluctuations in the VCI. This reflected that the variations in the wet and dry conditions of vegetation drought in Region A were more severe than those in other areas, primarily because of the climatic environment and geographical influences.

The changes in the monthly GDI of HP and its subregions from 2004 to 2022 are shown in Figure 5. As depicted in Figure 5, the GDI of HP and its subregions generally exhibited a decreasing trend, indicating a gradual exacerbation of GD. The period from 2004 to 2010 was mostly characterized by non-drought conditions. However, starting in 2011, the occurrence of GD became increasingly frequent, with the severity of drought intensifying annually. Furthermore, Regions A and B experienced similar changes in wetness and dryness, transitioning from a long-term wet state to a long-term dry state. Similarly, Regions C and D also shifted from wet to dry conditions overall, with some degree of alternating wetness and dryness in between.

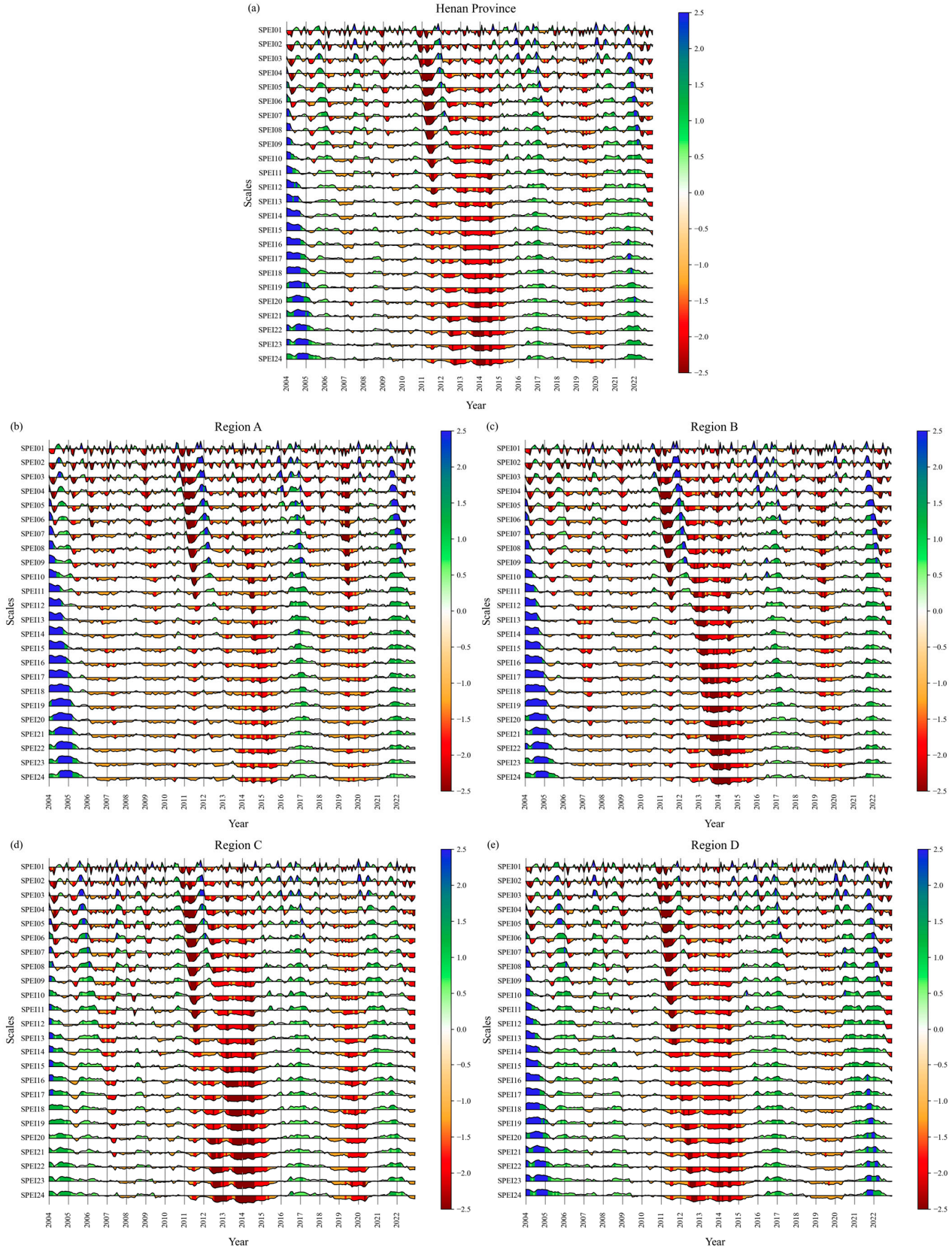

Figure 3. SPEI at the 1–24-month scales of Henan Province and its different subregions from 2004 to 2022 (calculated based on the entire region (**a**), Region A (**b**), Region B (**c**), Region C (**d**), and Region D (**e**)). The upper section of the horizontal axis represents wet conditions (blue), and the lower section represents dry conditions (red).

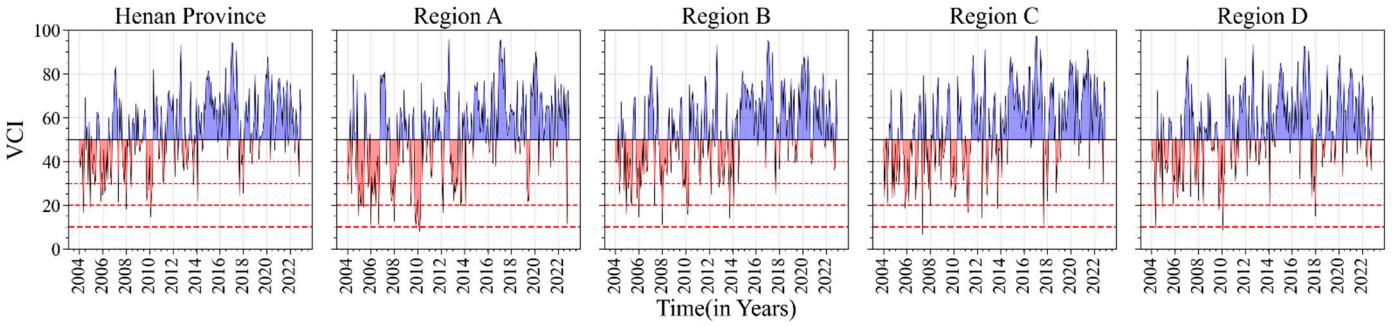

Figure 4. Temporal changes in the monthly VCI in Henan Province and its subregions during 2004–2022. The upper section of the horizontal axis represents wet conditions (blue), and the lower section represents dry conditions (red).

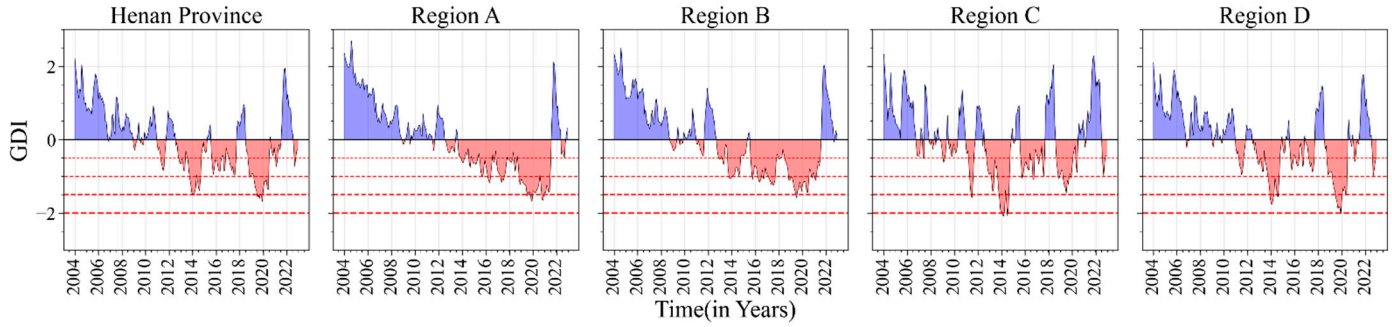

Figure 5. Temporal changes in the monthly GDI in Henan Province and its subregions during 2004–2022. The upper section of the horizontal axis represents wet conditions (blue), and the lower section represents dry conditions (red).

3.1.2. Spatial Distribution Characteristics of MD, AD, and GD

Figure 6 depicts the spatial distribution characteristics of MD, AD, and GD in HP during 2004–2022, including drought frequency, drought magnitude, drought duration, and drought severity. As illustrated in Figure 6a, there was a significant spatial difference in the distribution of MD frequency, with the highest occurrence in Region B in the northwest, followed by Region A, as well as localized occurrences in Regions C and D. Based on Figure 6b and Table 2, the spatial distribution of MD intensity averaged at 6.54, and did not exhibit significant differences. Figure 6c and Table 2 indicate that the overall duration of MD was 4.55 months, with relatively longer drought durations in the western part of the province. In terms of the severity of MD, as illustrated in Figure 6d, Regions A, B, and D exhibited higher severity compared to Region C, with Region A displaying the highest overall.

The spatial distribution of AD characteristics in HP from 2004 to 2022 is illustrated in Figure 6e–h. It is evident from Figure 6e that the frequency of AD occurrences was notably high across the entire province, with the northeastern region experiencing higher frequencies than the southwestern region. The distribution of drought magnitude depicted in Figure 6f indicated a higher magnitude in the eastern region compared to the western region. As shown in Figure 6g, it highlights prolonged drought durations in the northern and central parts of HP. Combined with Table 2, the average duration of AD province-wide was 8.70 months, which was twice the drought duration of MD. Furthermore, Figure 6h demonstrates that Region D exhibited the most severe agricultural drought, followed by Regions B and C, with Region A experiencing the lowest severity.

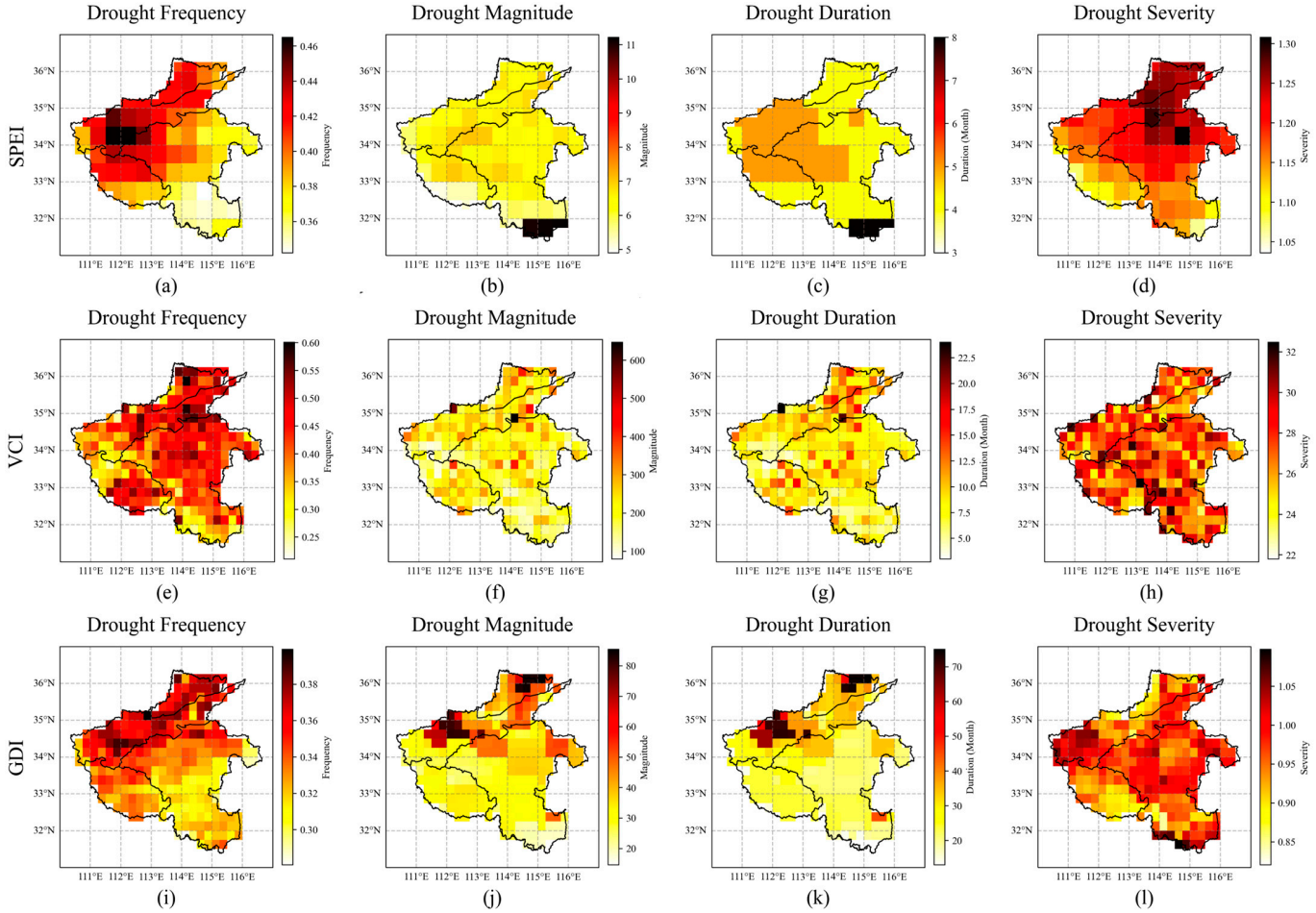

Figure 6. Spatial distribution of meteorological, agricultural, and groundwater drought characteristics based on the monthly SPEI (**a**–**d**), VCI (**e**–**h**), and GDI (**i**–**l**) in Henan Province during 2004–2022.

Table 2. Drought characteristics of meteorological, agricultural, and groundwater droughts in Henan Province and its subregions during 2004–2022.

Drought Type	Region	Drought Frequency	Drought Magnitude	Drought Duration	Drought Severity
MD	HP	0.40	6.54	4.55	1.19
	Region A	0.41	6.44	4.00	1.26
	Region B	0.43	6.45	4.60	1.21
	Region C	0.41	6.08	4.55	1.13
	Region D	0.38	6.74	4.61	1.19
AD	HP	0.42	211.88	8.70	27.43
	Region A	0.47	250.56	10.71	27.04
	Region B	0.43	231.77	9.51	27.28
	Region C	0.41	214.61	8.52	27.36
	Region D	0.42	195.37	8.05	27.58
GD	HP	0.34	37.33	29.03	0.97
	Region A	0.37	53.90	44.29	0.94
	Region B	0.36	45.62	38.81	0.98
	Region C	0.33	31.12	23.55	0.94
	Region D	0.33	32.71	23.67	0.98

According to Figure 6i, a clear north–south difference in the frequency of GD was observed in HP, with Regions A and B exhibiting the highest frequency while Regions C and D showed relatively lower. Figure 6j,k reveal that the spatial distribution characteristics of drought magnitude and drought duration for GD were similar to its drought frequency, being significantly higher in the northern part and lower in the southern part. Moreover, the average drought duration of GD in the entire province was 29.03 months, significantly exceeding that of both MD and AD (Table 2). Additionally, Figure 6l reveals that the drought severity in Regions B and D was higher than that in Regions A and C.

Figure 7 presents the drought frequency at different severity levels in MD, AD, and GD in HP and its subregions from 2004 to 2022. As shown in Figure 7a, the frequencies of mild and moderate drought levels in MD were relatively high, while severe and extreme droughts occurred less frequently. In comparison, Region A experienced the greatest number of drought events, while Region D experienced the least. According to Figure 7b, the frequency of mild drought levels was predominant in AD, with Region A experiencing more severe drought events than other regions. The data in Figure 7c exhibited that Region B experienced the greatest number of moderate drought events, closely followed by Region A. Conversely, Regions C and D encountered a greater number of severe and extreme drought events. Overall, it can be observed that the severity levels of MD events exceeded those of AD and GD, and multiple instances of extreme drought events occurred.

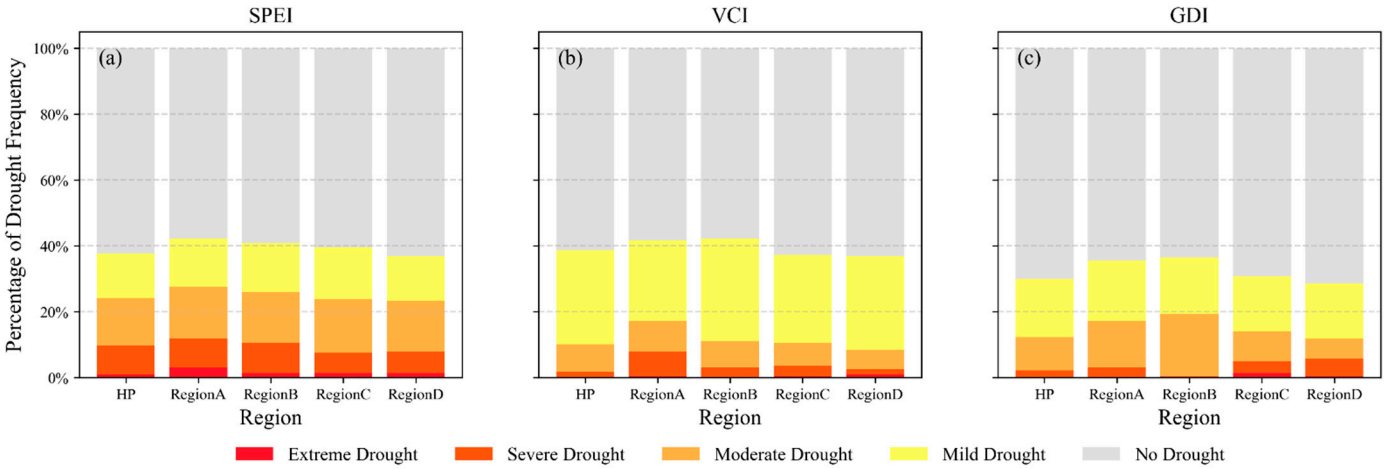

Figure 7. Drought frequency at different severity levels of meteorological, agricultural, and groundwater drought based on the monthly SPEI (**a**), VCI (**b**), and GDI (**c**) in Henan Province during 2004–2022.

3.2. Trend Identification of MD, AD, and GD

Sen's slope and MK trend test methods were used to further investigate the trends in the spatiotemporal variations in the SPEI, VCI, and GDI in HP from 2004 to 2022. As shown in Figure 8, noticeable spatial distribution differences were observed in the trends of the SPEI, VCI, and GDI across HP. Combined with Table 3, it can be observed that most of the regions exhibited increasing trends in both the SPEI and VCI. The area with an insignificant increasing trend in the SPEI accounted for 79.4%, while the areas with insignificant and significant increasing trends in the VCI accounted for 33.7% and 60.8%, respectively. This indicates that MD and AD were gradually alleviated in most areas of HP during the period from 2004 to 2022. However, there was a significant decreasing trend in the GDI accounting for 81.4%, indicating an aggravation of GD in HP.

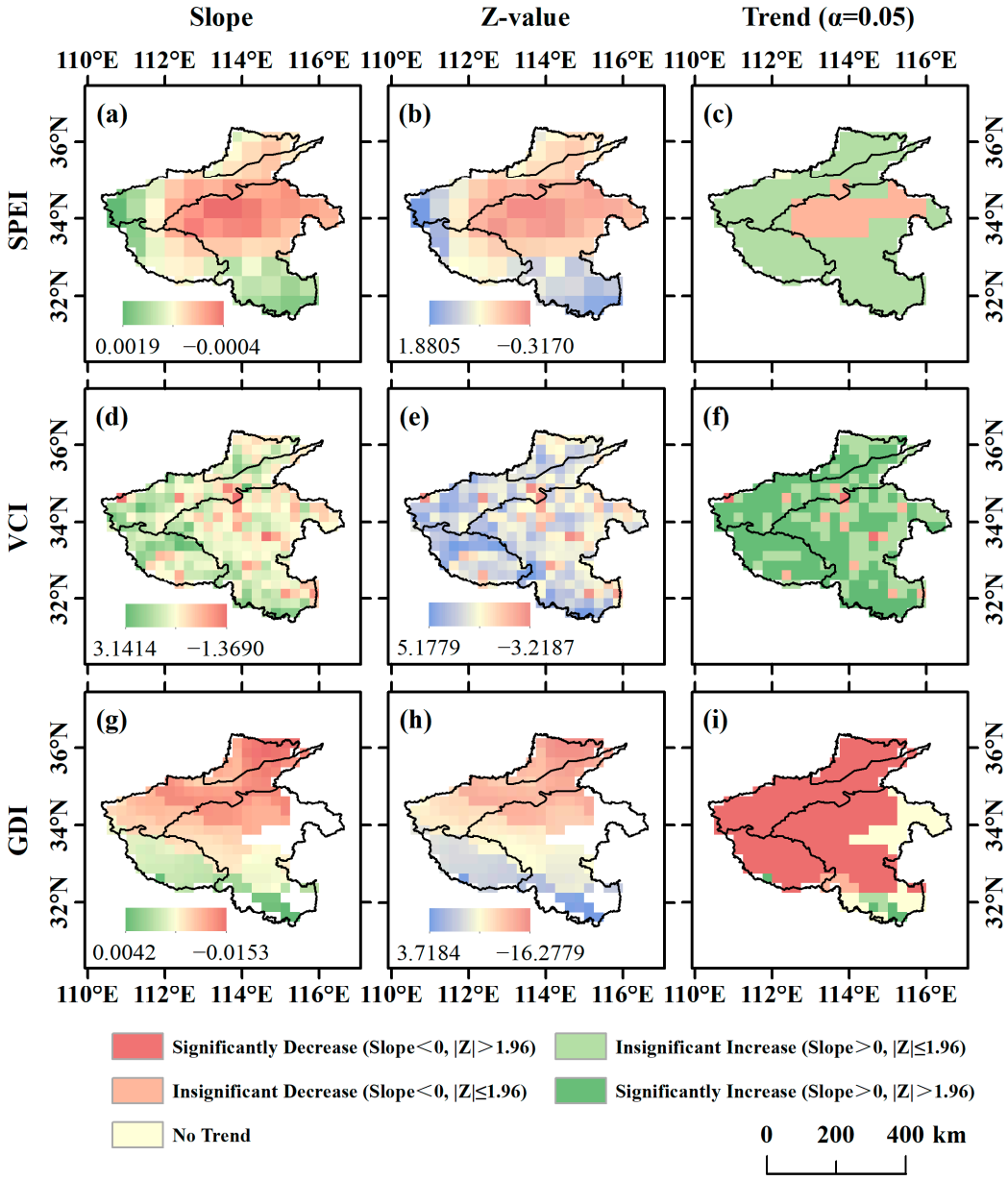

Figure 8. Spatial distributions of SPEI (**a**–**c**), VCI (**d**–**f**), and GDI (**g**–**i**) variation trends and significance tests in Henan Province from 2004 to 2022. From left to right, the three columns indicate the trend degree in Sen's slope estimate, the Z statistic from the MK test, and the superposition analysis of the first two.

Table 3. The percentages of areas of SPEI, VDI, and GDI in Henan Province from 2004 to 2022.

Drought Index	Significantly Decrease	Insignificant Decrease	No Trend	Insignificant Increase	Significantly Increase
SPEI	0	19.8%	0.8%	79.4%	0
VCI	1.2%	4.3%	0	33.7%	60.8%
GDI	79.1%	2.3%	15.1%	1.6%	1.9%

Based on Figure 8a–c, it is evident that the slope of the SPEI ranged from −0.0004 to 0.0019. Only the eastern region showed an insignificant decreasing trend, while the other areas exhibited an insignificant increasing trend. This indicated a pronounced exacerbation of MD in the northern part of Region D. Analysis of Figure 8d–f revealed that the slope of

the VCI varied between −1.3690 and 3.1414, with Z-values ranging from −3.2187 to 5.1779. Spatial variations and differences in distribution across the whole area were apparent. Nevertheless, AD across the province was gradually alleviated. Figure 8g–i demonstrate that the slope of the GDI ranged from −0.0153 to 0.0042, with Z-values falling between −16.2779 and 3.7184. GDI values were significantly decreasing across the entire province, except for minor increases or no changes in certain areas of Regions C and D, indicating a progressive worsening of GD. Furthermore, MD, AD, and GD in Region D tended to cluster, particularly MD and GD. However, this pattern was less pronounced in the other regions.

3.3. Propagation Dynamics of Droughts

3.3.1. Correlation and Propagation Time among MD, AD, and GD

As shown in Figure 9, there were significant spatial distribution differences in the correlation and propagation time of the three types of droughts (MD, AD, and GD) in HP. Figure 9a illustrates that the maximum correlation coefficients of the SPEI and VCI at the grid scale ranged from 0.06 to 0.30, with higher values in the west and lower values in the east of the province. This indicated a closer connection between MD and AD in the western region than in the eastern region. Similarly, the correlation between the SPEI and GDI was positive, and varied from 0.03 to 0.43 (Figure 9c). However, the spatial distribution of the correlation between the SPEI and GDI showed a pronounced north–south difference, suggesting a closer relationship between MD and GD in the southern part of HP. From Figure 9e, it can be observed that the correlation coefficient between the VCI and GDI ranged from −0.31 to 0.37, with a negative correlation in the northern part and a positive correlation in the southern part of HP, indicating that the correlation gradually increased from north to south. This difference was closely related to the spatial distribution of groundwater reserves in HP.

The spatial distributions of the propagation time among the three types of droughts in HP are illustrated in Figure 9b,d,f, indicating the shortest propagation time between the SPEI and VCI. As depicted in Figure 9b, the average drought propagation time from the SPEI to VCI in HP was 6.1 months, with that in Region A being 9.2 months, that in Region B being 5.4 months, that in Region C being 6.1 months, and that in Region D being 4.0 months (Table 4). Figure 9d displays the spatial distribution of the drought propagation time from the SPEI to GDI, revealing an average propagation time of 4.4 months from MD to GD, with the shortest of 1.0 months in Regions C and D, followed by 6.0 months in Region B, and the longest of 11.1 months in Region A (Table 4). Combined with Figure 9f and Table 4, the average drought propagation time from the VCI to GDI in HP was 16.3 months, with 19.5 months in Region A, 17.1 months in Region B, 14.1 months in Region C, and 18.5 months in Region D. Overall, there were significant spatial differences in the propagation time among MD, AD, and GD, primarily attributed to factors such as farmland distribution, human activities (artificial irrigation, etc.), and topography, which either accelerated or weakened the propagation of drought.

Table 4. Drought propagation time in Henan Province and its subregions during 2004–2022.

Region	MD to AD	MD to GD	AD to GD
HP	6.1	4.4	16.3
Region A	9.2	11.1	19.5
Region B	5.4	6.0	17.1
Region C	6.1	1.0	14.1
Region D	4.0	1.0	18.5

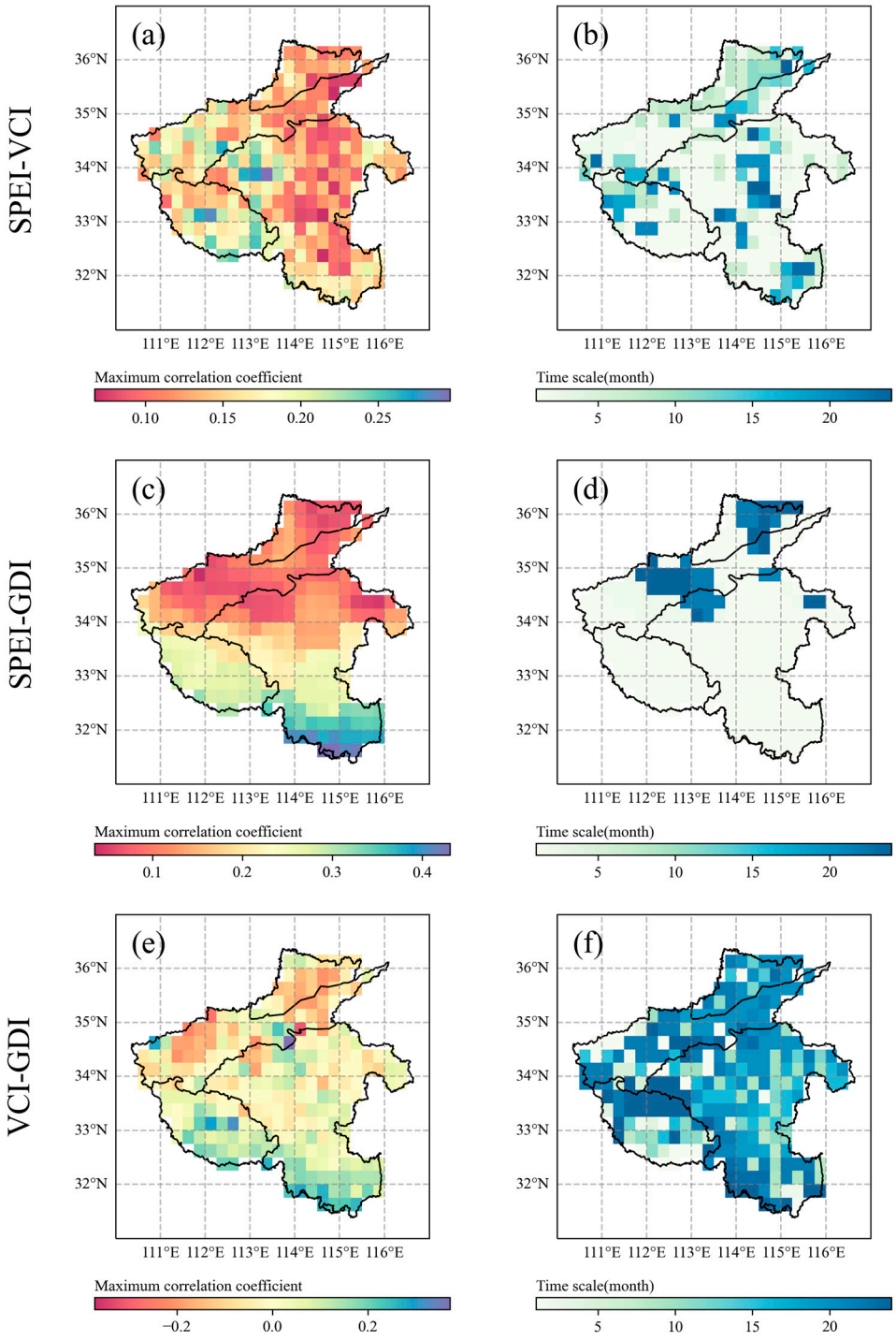

Figure 9. Spatial distributions of the maximum correlation coefficient (**a**,**c**,**e**) and propagation time (**b**,**d**,**f**) of SPEI-VCI (**a**,**b**), SPEI-GDI (**c**,**d**), and VCI-GDI (**e**,**f**) in Henan Province.

3.3.2. Seasonal Characteristics of Drought Propagation in Different Subregions

To further accurately analyze the correlation and propagation of MD, AD, and GD, as well as their distinctions among different climatic conditions in various subbasins of HP, the correlation coefficients between the SPEI-*n* (n = 1, 2, 3 . . . 24) and the monthly VCI and monthly GDI were calculated. Considering the varying responses of vegetation and groundwater to meteorological factors such as temperature, precipitation, and evapotranspiration across different months, it is necessary to study the propagation time from MD to AD and GD every month. As illustrated in Figure 10, the correlation between the SPEI and

GDI was higher than that between the SPEI and VCI, indicating a stronger linkage between MD and GD, whereas the relationship between MD and AD was relatively weaker.

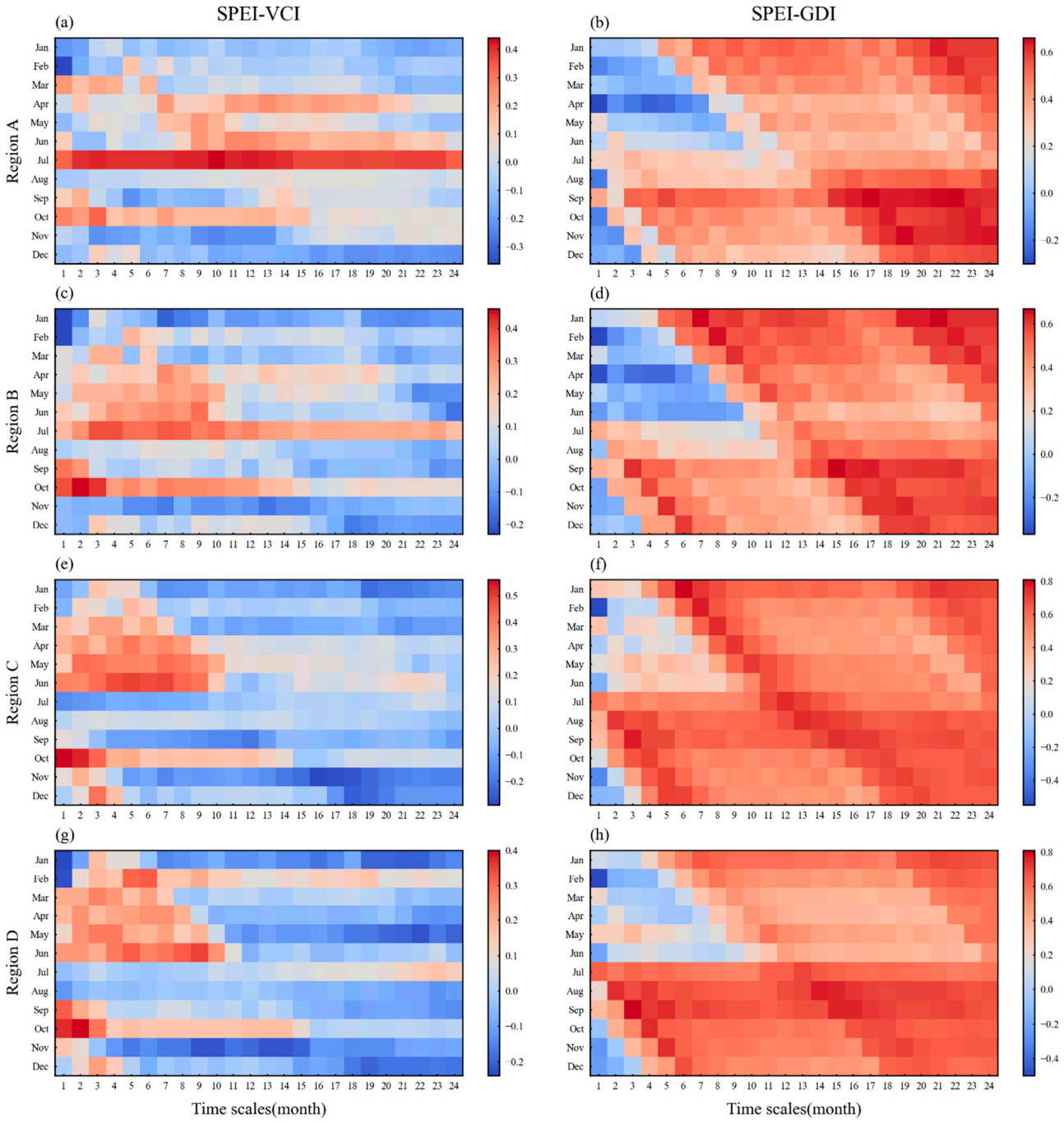

Figure 10. The correlation coefficients between SPEI-*n* (*n* = 1, 2, 3 . . . 24) and monthly VCI (**a**,**c**,**e**,**g**), SPEI-*n* (*n* = 1, 2, 3 . . . 24) and monthly GDI (**b**,**d**,**f**,**h**) of different subregions in Henan Province.

Figure 10 illustrates the seasonal and regional differences in the correlation between the SPEI-VCI and SPEI-GDI in various subregions, suggesting the influence of other factors on the hydrological cycle in these areas. As depicted in Figure 10a, the shortest drought propagation times occurred in March, July, and September–October (1–3 months). In particular, the VCI in July exhibited a strong correlation (0.33–0.44) with the SPEI at different time scales, indicating a propensity for MD to transition to AD during this month. This could be because of the high temperatures, limited precipitation, and strong evapotranspiration

during the summer, leading to vegetation water stress, and consequently shortening the propagation time of MD-AD. Figure 10c shows that the SPEI-VCI correlation in Region B was highest during the summer and autumn, followed by the spring, with a predominantly negative correlation in winter. The shortest propagation time of MD-AD occurred in July and September–October (1–4 months), while the longest occurred from April to June (7–9 months). As shown in Figure 10e, the propagation time of MD-AD in Region C was generally short, spanning from January to June (1–5 months) and from October to December (1–3 months), with the strongest correlation observed between SPEI01 and the monthly VCI in October, reaching 0.56. In Figure 10g, the shortest drought propagation period in Region D occurred from September to October (1–2 months), followed by February (5 months), and the longest occurred in June (9 months), indicating that meteorological factors (temperature, precipitation, evapotranspiration, etc.) play a role in shortening or extending the propagation time of MD-AD.

As shown in Figure 10b, the SPEI-GDI in Region A exhibited the strongest correlation in autumn, followed by that in winter, and weaker correlations in spring and summer. The shortest propagation time from MD to GD occurred between September and November (1–3 months), while the longest occurred between April and June (10–12 months). Additionally, there was a strong correlation (up to 0.66) between the GDI and the SPEI at different time scales in September. From September to November, characterized by high temperatures and low rainfall in the preceding summer months (e.g., July to August), intensified human activities (reservoir storage, groundwater extraction for crop irrigation, etc.), and high rates of evapotranspiration led to a reduction in groundwater storage, significantly shortening the propagation time from MD to GD. In Region B (Figure 10d), the period of drought propagation ranged from 7 to 9 months in spring, the shortest occurred in summer (July to August), about 1 to 2 months, and the longest occurred in June (12 months). In autumn, the propagation time ranged from 1 to 3 months, and in winter, from 4 to 6 months. Compared to other subregions, Region C (Figure 10f) exhibited the highest correlation coefficient between the SPEI and GDI, indicating a closer relationship between MD and GD, with GD responding more rapidly to MD. The propagation time from MD to GD in Region C was the shortest between July and September (1 month), the longest occurred in April (7 months), and those taking 2 to 6 months occurred in other months. In Figure 10h, the correlation between the SPEI and GDI in Region D was higher in the summer and autumn than in the spring and winter. The shortest drought propagation time occurred between July and October (1–2 months), with the longest duration occurring in June (12 months). Overall, Region C exhibited the highest correlation in terms of the SPEI-GDI, followed by Regions D and B, with Region A showing the lowest correlation.

3.4. Linkage Analysis Among MD, AD, and GD

In this study, XWT and WTC were utilized to explore the linkages among the SPEI-VCI, SPEI-GDI, and VCI-GDI. The results can be seen in Figures 11 and 12. In the graphical representations, the horizontal axis denotes the timeline of the time series, the vertical axis represents the changing periods, and the color indicates the intensity of these periods. The thin black solid line illustrates the Cone of Influence (COI) for the wavelet boundary effect, while the thick black solid line region represents the significant correlation through a red noise test at the 95% confidence level. Arrows are used to represent the phase relationship between the two: $\rightarrow$ denotes synchronous changes, indicating a positive correlation; $\downarrow$ indicates a 90° leading phase of the former sequence over the latter; $\leftarrow$ signifies an opposite phase, implying a negative correlation; and $\uparrow$ represents a 90° lagging phase of the former sequence behind the latter.

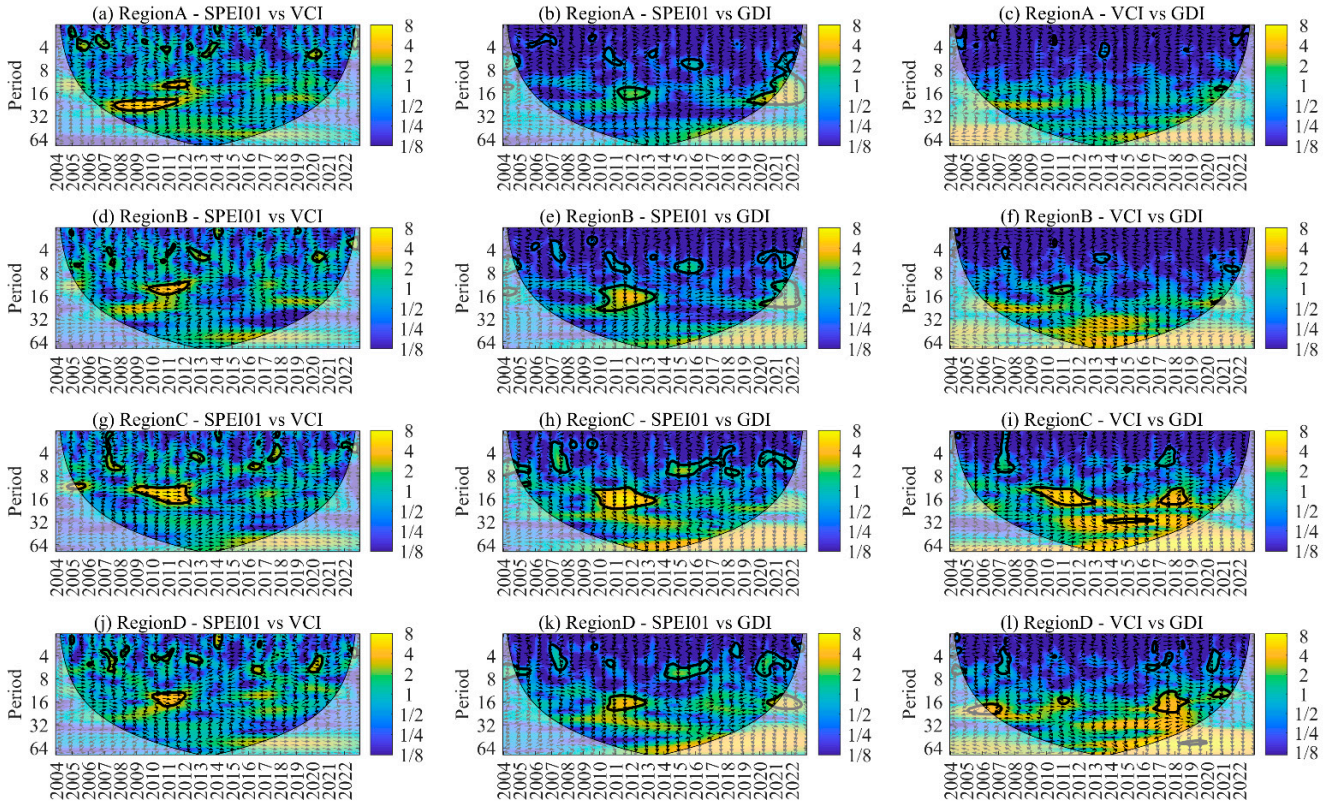

Figure 11. The cross-wavelet transform among monthly SPEI01, VCI, and GDI of different subregions in Henan Province. Region A (**a**–**c**), Region B (**d**–**f**), Region C (**g**–**i**), and Region D (**j**–**l**).

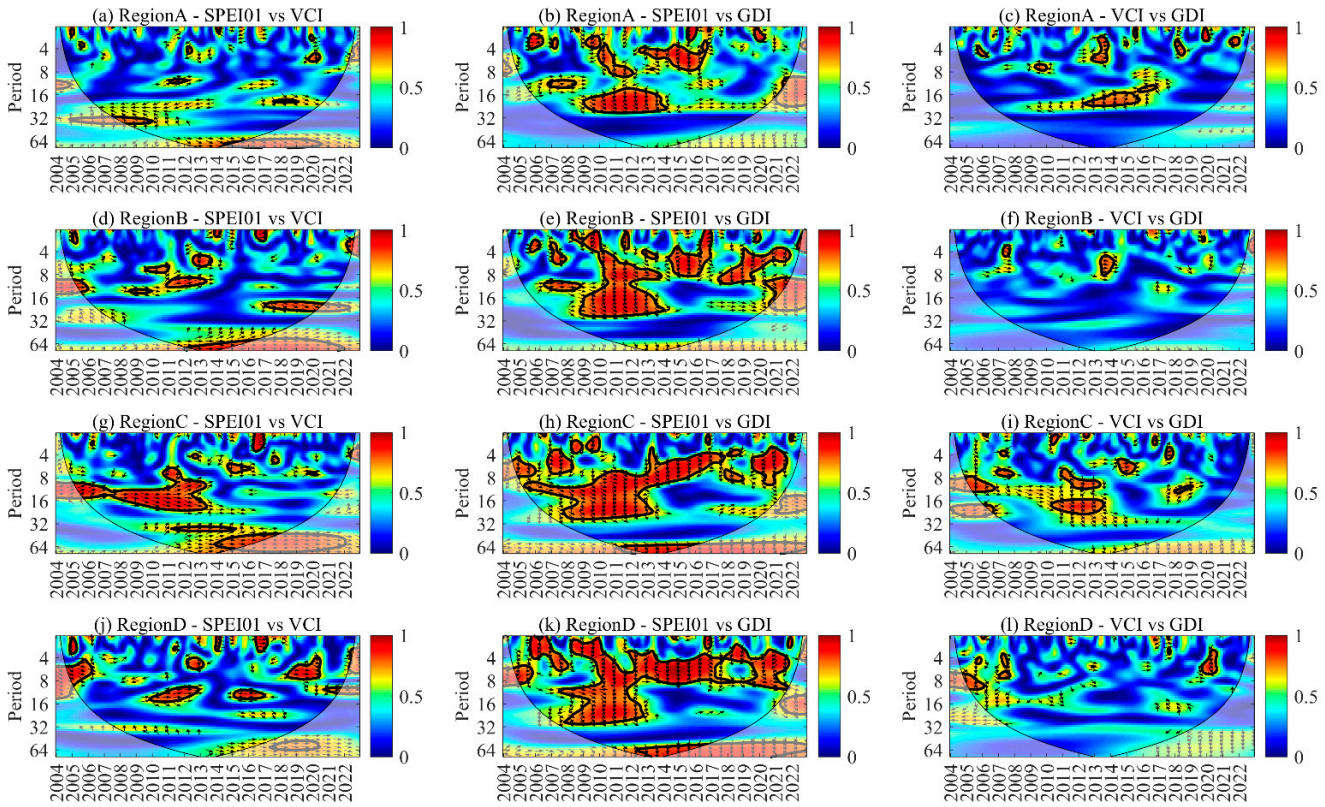

Figure 12. The wavelet coherence among monthly SPEI01, VCI, and GDI of different subregions in Henan Province. Region A (**a**–**c**), Region B (**d**–**f**), Region C (**g**–**i**), and Region D (**j**–**l**).

3.4.1. XWT Analysis

As shown in Figure 11, the impacts of climate change in different basins resulted in distinct differences in the high-energy resonance cycles, notable periods, and lag characteristics among MD, AD, and GD. There was a strong correlation between the SPEI and VCI in Region A. In the high-frequency domain, there were two resonance periods: one displaying a significant negative correlation over a time scale of 20–28 months (2007–2011), and the other showing a significant positive correlation at a time scale of 12–14 months in 2011 (Figure 11a). Although a resonance period of 6–24 months was observed for the SPEI-GDI from 2019 to 2022, it was heavily influenced by potential edge effects (Figure 11b). In Region B, a significant positive correlation was observed between the SPEI-VCI at the time scale of 12–16 months from 2010 to 2012 (Figure 11d), while the SPEI-GDI exhibited resonance periods of 12–24 months (2010–2013), with most phase angles close to 90°, indicating that the change in the SPEI occurred before the GDI during this period (Figure 11e). In Region C, the correlation between the SPEI-VCI was significantly positive at the time scale of 12–20 months from 2009 to 2012 (Figure 11g). The resonance period of the SPEI-GDI was observed from 2009 to 2013, indicating the SPEI's precedence over the GDI. Figure 11i illustrated three distinct resonance periods between the VCI and GDI, at 12–20 months (2009–2012), 30–32 months (2013–2016), and 12–20 months (2017–2018) time scales, but their phase variations differed, indicating that the VCI may lead or lag the GDI at different times. In Region D, the resonance periods for the SPEI-VCI and SPEI-GDI were similar to those in Region C. Additionally, the VCI and GDI were strongly linked in Region D, with two distinct resonance periods at 16–24 months (2006) and 12–24 months (2017–2018) (Figure 11l).

3.4.2. WTC Analysis

WTC was employed to further explore the coherence between different types of droughts in low- and high-energy regions (Figure 12), to elucidate the interrelationships among MD, AD, and GD. As shown in Figure 12, there was a significant difference in the relationships among different types of droughts. The coherence between MD and GD was the strongest, followed by that between MD and AD, and the weakest coherence was observed between AD and GD. Moreover, the strength of coherence among the three types of droughts varied across different subregions. In Region A, the relationship between the SPEI and VCI was relatively weak, with almost no discernible resonance periods (Figure 12a). However, as illustrated in Figure 12b, a close relationship was observed between the SPEI and GDI, exhibiting six distinct resonance periods: 3–4 months (2006, 2009), 4–10 months (2010–2011), 4–8 months (2012–2016), 12–14 months (2007–2008), and 14–32 months (2009–2014). Notably, in Regions B (Figure 12d–e), C (Figure 12g–h), and D (Figure 12j–k), the coherences between the SPEI-VCI and SPEI-GDI were stronger than those in Region A, indicating a pronounced consistency in the periodic variations in MD-AD and MD-GD. Additionally, in Region C, the VCI and GDI exhibited four relatively strong resonance periods (Figure 12i): 8–13 months (2005–2006), 7–12 months (2011–2013), 16–24 months (2010–2013), and 5–7 months (2014–2015), with an overall positive phase angle relationship, indicating that the VCI was ahead of the GDI.

4. Discussion

4.1. The Impact of Different Factors on the Propagation of Drought

Understanding the variations in influencing factors during the drought propagation process is crucial for unraveling the underlying mechanisms of drought propagation. As mentioned in Sections 3.3 and 3.4, there was a strong linkage between MD and AD/GD, but significant variations were evident across different subregions. Hence, it is imperative to further investigate how various factors such as climate variations, land surface conditions, and human activities influence the propagation among these three types of drought in different river basins [52]. In this study, nine variables relevant to drought propagation were considered, including precipitation (PRE), temperature (TEM), evapotranspiration

(ET), vegetation (NDVI), surface water resources (SWR), groundwater resources (GWR), the storage capacity of large and medium reservoirs (L/M-RSC), agricultural irrigation water consumption (AIWC), and total water consumption for industrial, urban and rural living, and environment (I-UR-E-TWC), thereby quantifying the influence of these factors during the drought propagation [42].

As shown in Figure 13, the raincloud plots illustrated the variations in the nine influencing factors in different subregions of HP from 2004 to 2022. Based on the violin plots, it can be observed that the distributions of these factors were uneven, with significant differences among the subregions. Combined with Figure 12, it was evident that factors such as climate change, surface conditions, and human activities in different river basins influenced the propagation of the three types of droughts. In Region A, low precipitation, high evaporation, and elevated mean annual temperatures led to frequent MD. As shown in Figure 12a, the propagation from MD to AD was not significant due to the region's minimal vegetation cover and agricultural irrigation. However, there was a close relationship between MD and GD, which could largely be attributed to the depletion of surface and groundwater reserves following MD, coupled with increased water consumption, exacerbating GD (Figure 12b). In Region B, Figure 12d,e showed a stronger connection between MD and AD/GD, influenced by factors such as surface water utilization, groundwater extraction, agricultural irrigation, and the development of water infrastructure [61,62]. These factors, as depicted in Figure 13, accelerated the propagation of drought, leading to a faster propagation from MD to AD and GD. In Region C, Figure 12d,e indicated the closest relationships between MD, AD, and GD. This region had the highest vegetation cover, and after MD, the threat to vegetation growth led to a decline in vegetation greenness and moisture content, triggering AD [63,64]. Intensive human activities further increased water consumption, disrupted the hydrological cycle, and accelerated the propagation from MD to GD [65]. Additionally, Figure 13 indicated that Region D had the most abundant water resources and vegetation cover. However, after the occurrence of MD, factors such as high temperatures and increased evaporation rates, along with a sharp rise in crop and human water demand, intensified water resource stress, shortening the propagation time from MD to AD and GD [10].

Therefore, it is essential to utilize water resources efficiently through integrated planning and management to strengthen drought resilience in HP. For Region A, given its low rainfall and limited groundwater resources, we recommend implementing groundwater recharge projects and improving groundwater management. Optimizing surface water storage and utilizing rainwater collection systems during frequent MD can mitigate resource shortages. Additionally, promoting water-efficient technologies will reduce agricultural water wastage. In Region B, where agricultural water demand is high, advanced irrigation techniques such as drip and sprinkler irrigation should be prioritized to minimize evaporation losses. Drought-resistant crops should be encouraged to reduce dependence on water during dry periods, and water infrastructure improvements should enhance resource allocation efficiency. For Region C, where human activities significantly influence drought propagation, it is crucial to protect the environment and promote water-saving technologies. Monitoring the hydrological cycle will ensure sustainable water use and slow the propagation from MD to AD and GD. Although Region D has abundant resources, high temperatures and evapotranspiration during droughts increase water demand, so better water storage management and pre-drought planning are necessary. Implementing drought warning systems will help prevent severe impacts on agriculture and ecosystems. In conclusion, we hope the results of this study can serve as a scientific reference for mitigating regional droughts, promoting sustainable agricultural and food production, and ensuring the effective management of water resources.

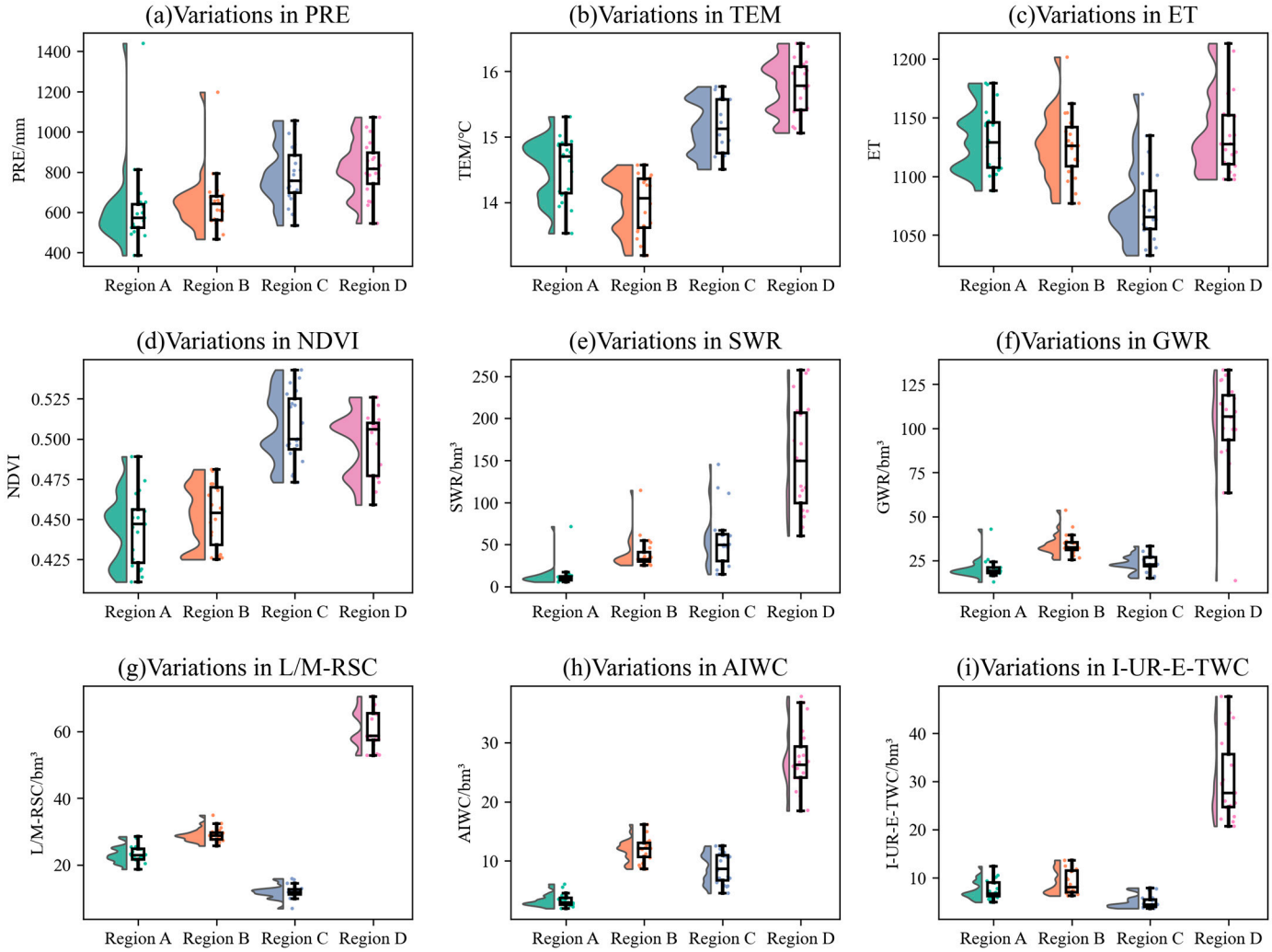

Figure 13. The variations in nine influential factors in drought propagation of different subregions in Henan Province from 2004 to 2022. (**a**–**i**) are precipitation (PRE), temperature (TEM), evapotranspiration (ET), vegetation (NDVI), surface water resources (SWR), groundwater resources (GWR), storage capacity of large and medium reservoirs (L/M-RSC), agricultural irrigation water consumption (AIWC), and total water consumption for industrial, urban and rural living, and environment (I-UR-E-TWC), respectively.

4.2. Uncertainties and Limitations of This Study

In this study, most of the selected research data were obtained and preprocessed based on GEE. Although GEE offers abundant spatiotemporally continuous environmental geographic data, the resolutions of the SPEIbase v2.9 [66] and GLDAS-2.2 [67] utilized in this study exhibited certain limitations, leading to a degree of uncertainty in regional drought studies [36]. Furthermore, this study only used statistical methods (run theory, PCC, XWT, and WTC) to unveil the propagation of droughts by capturing linear and nonlinear relationships, presenting certain limitations in comprehensively analyzing the propagation of drought [68]. Given the complexity of drought, the heterogeneity of events, and the impact of multiple factors including natural phenomena and human activities, further research is warranted to more deeply investigate the propagation dynamics of drought [1].

4.3. Advantages and Future Work

The majority of past studies have been concerned with comparisons between MD and AD (or HD) [48,58,69,70], with limited exploration into multiple types of droughts.

This study employed the SPEI, VCI, and GDI to identify the characteristics of MD, AD, and GD, respectively. This study revealed the propagation among these three types of droughts, providing new insights into regional drought propagation research. However, in HP, as a major agricultural region, intensive human activities (such as agricultural irrigation and groundwater extraction) significantly impacted the interrelations between AD and GD [68]. Consequently, future research should differentiate between irrigated agriculture and rainfed agriculture concerning their influence on regional drought propagation. Furthermore, droughts are influenced by various driving factors within the water cycle and energy cycle. In addition to the natural factors and human activities mentioned in this study, atmospheric circulation anomalies, land cover types, and land use should also be considered [71]. The quantitative analysis of factors influencing drought propagation can be facilitated by employing modeling techniques. In summary, future research on drought propagation should comprehensively consider meteorological, agricultural, hydrological, and socioeconomic droughts, analyze the underlying mechanisms throughout the entire drought process, and quantitatively assess the impacts of different driving factors.

5. Conclusions

In the context of current climate change, investigating the spatiotemporal characteristics, propagation dynamics, and primary influencing factors of droughts holds significant relevance for relevant authorities engaged in managing drought disasters, making reasonable decisions, and ensuring equitable allocation of water resources. In this study, HP and its four subregions were utilized as the research objects. We investigated the spatiotemporal characteristics and trends of MD, AD, and GD from 2004 to 2022 based on the SPEI, VCI, and GDI, and explored the correlations and propagation times among the three types of droughts under different climatic conditions. Additionally, we analyzed the interlinkages among the three types of droughts. The main conclusions are as follows:

(1) Significant disparities in spatial distribution were observed in MD, AD, and GD across HP. From 2004 to 2022, the average durations for these three types of droughts were 4.55 months, 8.70 months, and 29.03 months, respectively. Overall, MD events exhibited greater severity compared to AD and GD, reaching extreme drought levels several times.

(2) From 2004 to 2022, an increasing trend in the SPEI and VCI was evident in the majority of HP, suggesting a gradual alleviation of MD and AD conditions. Conversely, a significant decrease in the GDI was consistently observed across the province, indicating an exacerbation of GD.

(3) The correlations of MD-AD and MD-GD were positive, but with notable regional variations: the correlation of the SPEI-VCI was stronger in the west than in the east, while the correlation of the SPEI-GDI was stronger in the south than in the north. Moreover, the average propagation time of MD-AD was 6.1 months, that of MD-GD was 4.4 months, and that of AD-GD was 16.3 months.

(4) The propagation time of drought exhibited significant seasonality, being shorter in the summer and autumn compared to the winter and spring. For the propagation time of MD-AD, Region A experienced the shortest (1 months) in the summer (July), Region B spanned 1 to 4 months during summer and autumn, and in Region C, the shortest of that (1 months) occurred in the autumn (October). Similarly, Region D displayed the shortest propagation time in summer and autumn (1–2 months), with the longest time extending up to 9 months. Moreover, regarding MD-GD, all subregions were most prone to 1 to 3 months of propagation during autumn, especially in Region C, which was identified as a hotspot area for MD-GD.

(5) MD showed a close association with AD and GD. In Region C, these three types of droughts exhibited similar cyclical characteristics, resonance frequencies, and phase shift features. Consequently, the response relationships among these three types of droughts were comparatively strong in Region C.

Author Contributions: Conceptualization, H.X., R.Z. and Z.Y.; methodology, H.X. and R.Z.; software, R.Z.; validation, H.X., W.L. and Z.Y.; formal analysis, W.L.; investigation, W.L.; resources, H.X.; data curation, R.Z.; writing—original draft preparation, H.X. and R.Z.; writing—review and editing, H.X., R.Z., W.L. and Z.Y.; visualization, R.Z.; supervision, W.L. and Z.Y.; funding acquisition, H.X. and W.L. All authors have read and agreed to the published version of the manuscript.

Funding: This research was funded by the National Natural Science Foundation of China (No. 42201328), and the Key Scientific and Technological Project of Henan Province (No. 232102320247).

Institutional Review Board Statement: Not applicable.

Data Availability Statement: Data are contained within the article.

Conflicts of Interest: The authors declare no conflicts of interest.

References

1. West, H.; Quinn, N.; Horswell, M. Remote sensing for drought monitoring & impact assessment: Progress, past challenges and future opportunities. *Remote Sens. Environ.* **2019**, *232*, 111291. [CrossRef]
2. Zhang, H.; Ding, J.; Wang, Y.; Zhou, D.; Zhu, Q. Investigation about the correlation and propagation among meteorological, agricultural and groundwater droughts over humid and arid/semi-arid basins in China. *J. Hydrol.* **2021**, *603*, 127007. [CrossRef]
3. Su, B.; Huang, J.; Mondal, S.K.; Zhai, J.; Wang, Y.; Wen, S.; Gao, M.; Lv, Y.; Jiang, S.; Jiang, T.; et al. Insight from CMIP6 SSP-RCP scenarios for future drought characteristics in China. *Atmos. Res.* **2021**, *250*, 105375. [CrossRef]
4. Wan, L.; Bento, V.A.; Qu, Y.; Qiu, J.; Song, H.; Zhang, R.; Wu, X.; Xu, F.; Lu, J.; Wang, Q. Drought characteristics and dominant factors across China: Insights from high-resolution daily SPEI dataset between 1979 and 2018. *Sci. Total Environ.* **2023**, *901*, 166362. [CrossRef]
5. Zhang, X.; Hao, Z.; Singh, V.P.; Zhang, Y.; Feng, S.; Xu, Y.; Hao, F. Drought propagation under global warming: Characteristics, approaches, processes, and controlling factors. *Sci. Total Environ.* **2022**, *838*, 156021. [CrossRef]
6. Anshuka, A.; van Ogtrop, F.F.; Willem Vervoort, R. Drought forecasting through statistical models using standardised precipitation index: A systematic review and meta-regression analysis. *Nat. Hazards* **2019**, *97*, 955–977. [CrossRef]
7. Xu, Y.; Zhang, X.; Wang, X.; Hao, Z.; Singh, V.P.; Hao, F. Propagation from meteorological drought to hydrological drought under the impact of human activities: A case study in northern China. *J. Hydrol.* **2019**, *579*, 124147. [CrossRef]
8. Gao, C.; Liu, L.; Zhang, S.; Xu, Y.-P.; Wang, X.; Tang, X. Spatiotemporal patterns and propagation mechanism of meteorological droughts over Yangtze River Basin and Pearl River Basin based on complex network theory. *Atmos. Res.* **2023**, *292*, 106874. [CrossRef]
9. Apurv, T.; Cai, X. Drought Propagation in Contiguous U.S. Watersheds: A Process-Based Understanding of the Role of Climate and Watershed Properties. *Water Resour. Res.* **2020**, *56*, e2020WR027755. [CrossRef]
10. Geng, G.; Zhang, B.; Gu, Q.; He, Z.; Zheng, R. Drought propagation characteristics across China: Time, probability, and threshold. *J. Hydrol.* **2024**, *631*, 130805. [CrossRef]
11. Ramirez, A.R.; Crausbay, S.D.; Carter, S.L.; Cross, M.S.; Hall, K.R.; Bathke, D.J.; Betancourt, J.L.; Colt, S.; Cravens, A.E.; Dalton, M.S.; et al. Defining Ecological Drought for the Twenty-First Century. *Bull. Am. Meteorol. Soc.* **2017**, *98*, 2543–2550. [CrossRef]
12. Zhang, Z.; Lai, H.; Wang, F.; Feng, K.; Qi, Q.; Li, Y. Spatial–Temporal Patterns and Propagation Dynamics of Ecological Drought in the North China Plain. *Water* **2022**, *14*, 1542. [CrossRef]
13. Han, Z.; Huang, S.; Huang, Q.; Leng, G.; Wang, H.; Bai, Q.; Zhao, J.; Ma, L.; Wang, L.; Du, M. Propagation dynamics from meteorological to groundwater drought and their possible influence factors. *J. Hydrol.* **2019**, *578*, 124102. [CrossRef]
14. Cao, S.; Zhang, L.; He, Y.; Zhang, Y.; Chen, Y.; Yao, S.; Yang, W.; Sun, Q. Effects and contributions of meteorological drought on agricultural drought under different climatic zones and vegetation types in Northwest China. *Sci. Total Environ.* **2022**, *821*, 153270. [CrossRef]
15. Fawen, L.; Manjing, Z.; Yong, Z.; Rengui, J. Influence of irrigation and groundwater on the propagation of meteorological drought to agricultural drought. *Agric. Water Manag.* **2023**, *277*, 108099. [CrossRef]
16. Du, C.; Chen, J.; Nie, T.; Dai, C. Spatial–temporal changes in meteorological and agricultural droughts in Northeast China: Change patterns, response relationships and causes. *Nat. Hazards* **2021**, *110*, 155–173. [CrossRef]
17. Bevacqua, A.G.; Chaffe, P.L.B.; Chagas, V.B.P.; AghaKouchak, A. Spatial and temporal patterns of propagation from meteorological to hydrological droughts in Brazil. *J. Hydrol.* **2021**, *603*, 126902. [CrossRef]
18. Huang, S.; Huang, Q.; Chang, J.; Leng, G.; Xing, L. The response of agricultural drought to meteorological drought and the influencing factors: A case study in the Wei River Basin, China. *Agric. Water Manag.* **2015**, *159*, 45–54. [CrossRef]
19. Afshar, M.H.; Bulut, B.; Duzenli, E.; Amjad, M.; Yilmaz, M.T. Global spatiotemporal consistency between meteorological and soil moisture drought indices. *Agric. For. Meteorol.* **2022**, *316*, 108848. [CrossRef]
20. Fuentes, I.; Padarian, J.; Vervoort, R.W. Spatial and Temporal Global Patterns of Drought Propagation. *Front. Environ. Sci.* **2022**, *10*, 788248. [CrossRef]
21. Zhu, Y.; Liu, Y.; Wang, W.; Singh, V.P.; Ren, L. A global perspective on the probability of propagation of drought: From meteorological to soil moisture. *J. Hydrol.* **2021**, *603*, 126907. [CrossRef]

22. Bhardwaj, K.; Shah, D.; Aadhar, S.; Mishra, V. Propagation of Meteorological to Hydrological Droughts in India. *J. Geophys. Res. Atmos.* **2020**, *125*, e2020JD033455. [CrossRef]
23. Das, S.; Das, J.; Umamahesh, N.V. A Non-Stationary Based Approach to Understand the Propagation of Meteorological to Agricultural Droughts. *Water Resour. Manag.* **2022**, *37*, 2483–2504. [CrossRef]
24. Ding, Y.; Xu, J.; Wang, X.; Cai, H.; Zhou, Z.; Sun, Y.; Shi, H. Propagation of meteorological to hydrological drought for different climate regions in China. *J. Environ. Manag.* **2021**, *283*, 111980. [CrossRef]
25. Sun, P.; Liu, R.; Yao, R.; Shen, H.; Bian, Y. Responses of agricultural drought to meteorological drought under different climatic zones and vegetation types. *J. Hydrol.* **2023**, *619*, 129305. [CrossRef]
26. Dai, M.; Huang, S.; Huang, Q.; Zheng, X.; Su, X.; Leng, G.; Li, Z.; Guo, Y.; Fang, W.; Liu, Y. Propagation characteristics and mechanism from meteorological to agricultural drought in various seasons. *J. Hydrol.* **2022**, *610*, 127897. [CrossRef]
27. Li, Z.Y.; Huang, S.Z.; Zhou, S.; Leng, G.Y.; Liu, D.F.; Huang, Q.; Wang, H.; Han, Z.M.; Liang, H. Clarifying the Propagation Dynamics from Meteorological to Hydrological Drought Induced by Climate Change and Direct Human Activities. *J. Hydrometeorol.* **2021**, *22*, 2359–2378. [CrossRef]
28. Wang, J.; Wang, W.; Cheng, H.; Wang, H.; Zhu, Y. Propagation from Meteorological to Hydrological Drought and Its Influencing Factors in the Huaihe River Basin. *Water* **2021**, *13*, 1985. [CrossRef]
29. Xu, Z.; Wu, Z.; Shao, Q.; He, H.; Guo, X. From meteorological to agricultural drought: Propagation time and probabilistic linkages. *J. Hydrol. Reg. Stud.* **2023**, *46*, 101329. [CrossRef]
30. Wan, F.; Zhang, F.; Wang, Y.; Peng, S.; Zheng, X. Study on the propagation law of meteorological drought to hydrological drought under variable time Scale: An example from the Yellow River Water Supply Area in Henan. *Ecol. Indic.* **2023**, *154*, 110873. [CrossRef]
31. Rodell, M.; Houser, P.R.; Jambor, U.; Gottschalck, J.; Mitchell, K.; Meng, C.-J.; Arsenault, K.; Cosgrove, B.; Radakovich, J.; Bosilovich, M.; et al. The Global Land Data Assimilation System. *Bull. Am. Meteorol. Soc.* **2004**, *85*, 381–394. [CrossRef]
32. Vicente-Serrano, S.M.; Beguería, S.; López-Moreno, J.I. A Multiscalar Drought Index Sensitive to Global Warming: The Standardized Precipitation Evapotranspiration Index. *J. Clim.* **2010**, *23*, 1696–1718. [CrossRef]
33. Zhu, K.; Xu, Y.; Lu, F.; Sun, X.; Gao, M.; Han, X.; Li, D.; Jiang, M. Spatio-Temporal Evolution and Propagation of Meteoro-Hydrological Drought in Yalong River Basin. *Water* **2023**, *15*, 1025. [CrossRef]
34. Park, S.; Im, J.; Jang, E.; Rhee, J. Drought assessment and monitoring through blending of multi-sensor indices using machine learning approaches for different climate regions. *Agric. For. Meteorol.* **2016**, *216*, 157–169. [CrossRef]
35. Chu, H.; Venevsky, S.; Wu, C.; Wang, M. NDVI-based vegetation dynamics and its response to climate changes at Amur-Heilongjiang River Basin from 1982 to 2015. *Sci. Total Environ.* **2019**, *650*, 2051–2062. [CrossRef]
36. Gao, S.; Lai, H.; Wang, F.; Qiang, X.; Li, H.; Di, D. An Analysis of Spatial–Temporal Evolution and Propagation Features of Vegetation Drought in Different Sub-Zones of China. *Agronomy* **2023**, *13*, 2101. [CrossRef]
37. Kogan, F.N. Application of vegetation index and brightness temperature for drought detection. *Adv. Space Res.* **1995**, *15*, 91–100. [CrossRef]
38. Zambrano, F.; Lillo-Saavedra, M.; Verbist, K.; Lagos, O. Sixteen Years of Agricultural Drought Assessment of the BioBío Region in Chile Using a 250 m Resolution Vegetation Condition Index (VCI). *Remote Sens.* **2016**, *8*, 530. [CrossRef]
39. Agutu, N.O.; Awange, J.L.; Zerihun, A.; Ndehedehe, C.E.; Kuhn, M.; Fukuda, Y. Assessing multi-satellite remote sensing, reanalysis, and land surface models' products in characterizing agricultural drought in East Africa. *Remote Sens. Environ.* **2017**, *194*, 287–302. [CrossRef]
40. Thomas, B.F.; Famiglietti, J.S.; Landerer, F.W.; Wiese, D.N.; Molotch, N.P.; Argus, D.F. GRACE Groundwater Drought Index: Evaluation of California Central Valley groundwater drought. *Remote Sens. Environ.* **2017**, *198*, 384–392. [CrossRef]
41. Wang, F.; Wang, Z.; Yang, H.; Di, D.; Zhao, Y.; Liang, Q. Utilizing GRACE-based groundwater drought index for drought characterization and teleconnection factors analysis in the North China Plain. *J. Hydrol.* **2020**, *585*, 124849. [CrossRef]
42. Zhao, A.; Xiang, K.; Zhang, A.; Zhang, X. Spatial-temporal evolution of meteorological and groundwater droughts and their relationship in the North China Plain. *J. Hydrol.* **2022**, *610*, 127903. [CrossRef]
43. Liu, Y.; Shan, F.; Yue, H.; Wang, X.; Fan, Y. Global analysis of the correlation and propagation among meteorological, agricultural, surface water, and groundwater droughts. *J. Environ. Manag.* **2023**, *333*, 117460. [CrossRef] [PubMed]
44. Wang, F.; Lai, H.; Li, Y.; Feng, K.; Zhang, Z.; Tian, Q.; Zhu, X.; Yang, H. Identifying the status of groundwater drought from a GRACE mascon model perspective across China during 2003–2018. *Agric. Water Manag.* **2022**, *260*, 107251. [CrossRef]
45. Yevjevich, V.M. *An Objective Approach to Definitions and Investigations of Continental Hydrologic Droughts*; Colorado State University: Fort Collins, CO, USA, 1967; p. 23.
46. Chen, N.; Li, R.; Zhang, X.; Yang, C.; Wang, X.; Zeng, L.; Tang, S.; Wang, W.; Li, D.; Niyogi, D. Drought propagation in Northern China Plain: A comparative analysis of GLDAS and MERRA-2 datasets. *J. Hydrol.* **2020**, *588*, 125026. [CrossRef]
47. Wang, H.; Zhu, Y.; Qin, T.; Zhang, X. Study on the propagation probability characteristics and prediction model of meteorological drought to hydrological drought in basin based on copula function. *Front. Earth Sci.* **2022**, *10*, 961871. [CrossRef]
48. Zou, R.; Yin, Y.X.; Wang, X.J.; Zhang, Z.X.; Ma, X.Y.; Liu, M.Y.; Ullan, I. Characteristics and propagation of meteorological and hydrological droughts in eastern Gansu, a typical semi-arid region, China. *Int. J. Climatol.* **2023**, *43*, 5327–5347. [CrossRef]
49. Sen, P.K. Estimates of the regression coefficient based on Kendall's tau. *J. Am. Stat. Assoc.* **1968**, *63*, 1379–1389. [CrossRef]

50. Zhou, Z.; Shi, H.; Fu, Q.; Li, T.; Gan, T.Y.; Liu, S. Assessing spatiotemporal characteristics of drought and its effects on climate-induced yield of maize in Northeast China. *J. Hydrol.* **2020**, *588*, 125097. [CrossRef]
51. Mann, H.B. Nonparametric tests against trend. *Econom. J. Econom. Soc.* **1945**, *13*, 245–259. [CrossRef]
52. Huang, S.; Zhang, X.; Chen, N.; Li, B.; Ma, H.; Xu, L.; Li, R.; Niyogi, D. Drought propagation modification after the construction of the Three Gorges Dam in the Yangtze River Basin. *J. Hydrol.* **2021**, *603*, 127138. [CrossRef]
53. Pearson, K. VII. Note on regression and inheritance in the case of two parents. *Proc. R. Soc. Lond.* **1895**, *58*, 240–242.
54. Sun, S.; Li, Q.; Li, J.; Wang, G.; Zhou, S.; Chai, R.; Hua, W.; Deng, P.; Wang, J.; Lou, W. Revisiting the evolution of the 2009–2011 meteorological drought over Southwest China. *J. Hydrol.* **2019**, *568*, 385–402. [CrossRef]
55. Hudgins, L.; Friehe, C.A.; Mayer, M.E. Wavelet transforms and atmopsheric turbulence. *Phys. Rev. Lett.* **1993**, *71*, 3279. [CrossRef] [PubMed]
56. Torrence, C.; Compo, G.P. A practical guide to wavelet analysis. *Bull. Am. Meteorol. Soc.* **1998**, *79*, 61–78. [CrossRef]
57. Hudgins, L.; Huang, J. Bivariate wavelet analysis of Asia monsoon and ENSO. *Adv. Atmos. Sci.* **1996**, *13*, 299–312. [CrossRef]
58. Lin, H.; Yu, Z.B.; Chen, X.G.; Gu, H.H.; Ju, Q.; Shen, T.Q. Spatial-temporal dynamics of meteorological and soil moisture drought on the Tibetan Plateau: Trend, response, and propagation process. *J. Hydrol.* **2023**, *626*, 130211. [CrossRef]
59. Agarwal, A.; Maheswaran, R.; Kurths, J.; Khosa, R. Wavelet Spectrum and Self-Organizing Maps-Based Approach for Hydrologic Regionalization -a Case Study in the Western United States. *Water Resour. Manag.* **2016**, *30*, 4399–4413. [CrossRef]
60. Kang, Y.; Guo, E.; Wang, Y.; Bao, Y.; Bao, Y.; Mandula, N.; Runa, A.; Gu, X.; Jin, L. Characterisation of compound dry and hot events in Inner Mongolia and their relationship with large-scale circulation patterns. *J. Hydrol.* **2022**, *612*, 128296. [CrossRef]
61. Xu, Y.; Zhang, X.; Hao, Z.; Singh, V.P.; Hao, F. Characterization of agricultural drought propagation over China based on bivariate probabilistic quantification. *J. Hydrol.* **2021**, *598*, 126194. [CrossRef]
62. Zhang, Y.; Hao, Z.; Feng, S.; Zhang, X.; Xu, Y.; Hao, F. Agricultural drought prediction in China based on drought propagation and large-scale drivers. *Agric. Water Manag.* **2021**, *255*, 107028. [CrossRef]
63. Li, R.; Chen, N.; Zhang, X.; Zeng, L.; Wang, X.; Tang, S.; Li, D.; Niyogi, D. Quantitative analysis of agricultural drought propagation process in the Yangtze River Basin by using cross wavelet analysis and spatial autocorrelation. *Agric. For. Meteorol.* **2020**, *280*, 107809. [CrossRef]
64. Wang, F.; Lai, H.; Li, Y.; Feng, K.; Tian, Q.; Guo, W.; Zhang, W.; Di, D.; Yang, H. Dynamic variations of terrestrial ecological drought and propagation analysis with meteorological drought across the mainland China. *Sci. Total Environ.* **2023**, *896*, 165314. [CrossRef] [PubMed]
65. Liu, Y.; Shan, F.; Yue, H.; Wang, X. Characteristics of drought propagation and effects of water resources on vegetation in the karst area of Southwest China. *Sci. Total Environ.* **2023**, *891*, 164663. [CrossRef]
66. Beguería, S.; Serrano, S.M.V.; Reig-Gracia, F.; Garcés, B.L. SPEIbase v.2.9 [Dataset]. 2023. Available online: https://digital.csic.es/handle/10261/332007 (accessed on 1 February 2024).
67. Li, B.; Rodell, M.; Kumar, S.; Beaudoing, H.K.; Getirana, A.; Zaitchik, B.F.; de Goncalves, L.G.; Cossetin, C.; Bhanja, S.; Mukherjee, A.; et al. Global GRACE Data Assimilation for Groundwater and Drought Monitoring: Advances and Challenges. *Water Resour. Res.* **2019**, *55*, 7564–7586. [CrossRef]
68. Nigatu, Z.M.; You, W.; Melesse, A.M. Drought Dynamics in the Nile River Basin: Meteorological, Agricultural, and Groundwater Drought Propagation. *Remote Sens.* **2024**, *16*, 919. [CrossRef]
69. Li, Y.; Huang, S.; Wang, H.; Zheng, X.; Huang, Q.; Deng, M.; Peng, J. High-resolution propagation time from meteorological to agricultural drought at multiple levels and spatiotemporal scales. *Agric. Water Manag.* **2022**, *262*, 107428. [CrossRef]
70. Zhou, Z.; Shi, H.; Fu, Q.; Ding, Y.; Li, T.; Wang, Y.; Liu, S. Characteristics of Propagation From Meteorological Drought to Hydrological Drought in the Pearl River Basin. *J. Geophys. Res. Atmos.* **2021**, *126*, e2020JD033959. [CrossRef]
71. Zhou, K.; Li, J.; Zhang, T.; Kang, A. The use of combined soil moisture data to characterize agricultural drought conditions and the relationship among different drought types in China. *Agric. Water Manag.* **2021**, *243*, 106479. [CrossRef]